# THREE-DIMENSIONAL MULTIMEDIUM COMPUTATIONAL MODEL FOR DRUG DELIVERY USING FINITE ELEMENT ANALYSIS

by

EDUARDO MARTINEZ

Presented to the Faculty of the Graduate School of

The University of Texas at Arlington in Partial Fulfillment

of the Requirements

for the Degree of

MASTER OF SCIENCE IN BIOMEDICAL ENGINEERING

THE UNIVERSITY OF TEXAS AT ARLINGTON

May 2011

ACKNOWLEDGEMENTS

It is very difficult to express how grateful I am to the people that contributed to the development of this project.

First, I would like to thank Dr. Mario Romero-Ortega for supporting an idea outside his primary interest and supporting me and giving me the opportunity to work under his mentorship. His mentoring has helped me to learn new skills and has inspired the good academic character and integrity. Additionally, I appreciate the help of Dr. Saibun Tjuatja for his detail attention and insightful comments during the development of the computational models.

I would like to thank Dr.Kytai T. Nguyen and Dr. Saibun Tjuatja for serving in my committee and sharing their knowledge.

I thank all the members of my lab: Bich Pham, Nivedita Khobragade, Sarita Bhetawal, Tabasum Musa, Tarik Shihabeddin, Vidhi Desai, Collins Watson, Jennifer Bell, An Nguyen, Rozita Shafabakhsh and Brad Elmer for their support and friendship. I am especially grateful to Parisa Lofti for helping me define my project, Swarup Dash for answering questions and Dr. Jennifer L. Seifer for helping me with the thesis write up.

Finally, I wish to acknowledge my father Francisco Martinez, my mother Maria del Rocio Sanchez, and my siblings Rocio, Virgilio, Gabriel, and my girlfriend Veronica Mendez for their patience understanding and love during my academic career.

April 11, 2011

ABSTRACT

THREE-DIMENSIONAL MULTIMEDIUM COMPUTATIONAL MODEL FOR DRUG DELIVERY USING FINITE ELEMENT ANALYSIS

Eduardo Martinez, M.S.

The University of Texas at Arlington, 2011

Supervising Professor: Mario Romero-Ortega

Approximately 2.8% of trauma patients present peripheral nerve injury, which can result in loss of motor function. Current strategies for peripheral nerve repair had focused on the development of synthetic nerve conduits that provide physical guidance. One advantage of the synthetic nerve conduits is that the conduit can be utilize as a delivery system and gain the ability to deliver neurotrophic factors, which have an effect on controlling the survival, migration, proliferation, and differentiation of different neural cell types. Currently there is no method to quantify the concentration of growth factors in the nerve conduit during the implantation time.

In order to generate a spatiotemporal profile for the implantable rug delivery device, a complex multimedium model contemplating the release from polymers and diffusion in hydrogels, was developed. The model is based on two configurations of cylindrical nerve conduits that incorporated different hydrogels with and without the release from biodegradable polymer loaded microparticles. The hydrogel diffusion model was validated using published exact solutions for a cylinder and a sphere under perfect sink conditions. The calculated release profiles have a good agreement with the exact solutions with correlation coefficients of $R^2 = .995$ for the cylinder and $R^2 = .996$ for the sphere.

The release model based on microparticles was compared with the measured release of Pleiotrophin (PTN) loaded 50/50 Poly (lactide-co-glycolide) (PLGA) microparticles, showing a

correlation coefficient of $R^2 = .995$. The model was implemented for a period of 30 days and produced spatiotemporal concentrations for the lumen of the modeled devices. Simulation of implantable drug delivery devices will contribute significantly to the development of tissue engineering, making possible the determination of the spatiotemporal concentrations of biomolecules that could not be determined otherwise. The control of microenvironments could lead to the improvement of the development of implantable scaffolds in the areas of angiogenesis, vascularization, and regeneration of nerve and bone, among others.

TABLE OF CONTENTS

LIST OF ILLUSTRATIONS

Figure Page

LIST OF TABLES

# CHAPTER 1

# INTRODUCTION

## 1.1 Drug Delivery

Since the 1970s, the increased understanding of mechanisms of action of many drugs, led to the development of new classes of drug agents such as chimeric antibodies, peptides and virus like particles, among others[1]. The delivery of these new drug agents to a specific tissue target represents a challenge. Methods such as pills or injections are inadequate for delivery of some of the newly developed agents such as recombinant proteins that have a short half life, and might be toxic when delivered systemically [1, 2]. Drug delivery systems have the potential for administration of agents to specific tissue targets at specific concentrations, thus reducing the potential harmful effects of the drug in other tissues. Furthermore, specific delivery can increase drug bioavailability, and reduce the dosing frequency by controlling the release of the drug over long periods of time.

In controlled delivery the drug like molecule is combined with other component to produce a delivery system. Sustained release is achieved by mixing the drug molecule with excipients such as biocompatible polymers that alter the rate of release [1]. Polymers have been used for experimental drug delivery for long time and lately a few polymer based delivery systems such as: Estradiol/poly[ethylene-co-(vinyl acetate)], BCNU/poly[carboxyphenoxy-propane-co-(sebacic acid)], and Levonorgestrel/silicone elastomer among others, have been approved fro human use [1].

The advances in polymer technology have made possible the creation of sustain and even programmable delivery systems that incorporate different drug delivery modalities such as reservoir, matrix, hydrogel, and degradable delivery [3, 4]. Reservoir systems that release of drug from the reservoir into the external medium diffusing drug across a polymer membrane. Hydrogels, polymeric networks that

swell and retain aqueous solutions, are capable of immobilizing and maintaining the activity of proteins and drug molecules [5]. Degradable polymers are capable of incorporating drug molecules in their matrix and releasing them as the polymers are degraded into monomers. The release rate can be tailored for the requirements of the drug delivery by changing the physicochemical properties of the polymer [6].Changing the polymer type, molecular weight, monomer structure, and blending of polymers can alter these properties [3]. The incorporation of the polymer technology in drug delivery systems represents a breakthrough in the development of drug delivery technology.

### *1.1.1 Drug Delivery Systems for Peripheral Nerve Repair*

Approximately 2.8% of trauma patients present peripheral nerve injury, which can result in loss of motor function [46]. Peripheral nerve injury is not limited to trauma patients. Diseases and congenital defects are sources of peripheral nerve injury. Neurofibrosarcoma, a form of cancer that affects the connective tissue in the peripheral nerve, accounts fro approximately 200 thousand cases per year [46]. Current treatment for peripheral nerve injury consists in the surgical end to end reconnection of the damaged nerve; however, this procedure is only successful for short gap repair [46]. For longer gaps the golden standard is the use of an analogous nerve graft.

The analogous nerve grafts have disadvantages such as the need to perform more than one surgery and the loss of function at the donor site [46]. Current strategies for peripheral nerve repair had focused on the development of synthetic nerve conduits that provide physical guidance using a variety of synthetic materials such as polyester like such as poly(glycolic acid) (PGA), poly(lactic acid) (PLA), and poly(lactic-co-glycolic acid) (PLGA) [46]. Dr. Mario Romero's lab and others have proposed tabularization techniques that mimic the multifascicular nerve anatomy as well as increase the surface area of a nerve conduit [40]. The need for a nerve conduits that can mimic the microenvironment of a natural nerve bundle such as multiple channels, incorporation of growth factors, and control permeability to name a few are essential in regeneration. Nerve conduits can be used as drug delivery device to deliver neurotrophic factors, which have an effect on controlling the survival, migration, proliferation, and differentiation of

different neural cell types. The control of the concentration in the nerve conduit is imperative to obtain the desired biological effect.

The drug delivery system performance is dictated by the chemical and physical characteristics of the different materials involved in it. The testing of drug delivery systems is critical for the evaluation of the performance of the device, and for revealing potential flaws in the design. In the recent past, drug delivery systems have been tested experimentally, commonly using animal models [7]. Repeated testing for flaws in the system design leads to increasing cost and time for the development of the systems. However a quantitative understanding of the processes involved in drug delivery has led to the implementation of mathematical models. Several research areas have taken advantage of mathematical computer modeling to evaluate the performance of developed devices prior to fabrication and reducing significantly the time for development and optimization[8, 9].

## 1.2 Physical Phenomena Involved in Drug Delivery

### *1.2.1 Diffusion*

The transport of mass, energy, and momentum are governed by physical laws, based on a driving potential. The driving force is expressed as the gradient of the potential in the direction of flow. In the case of mass transfer, the rate law based on gradients is determined by Fick's Law, that states that the driving force involved in the transfer of mass is the molar concentration ($\phi$) in units of mol/m^3 as molecules diffuse from high to low concentration. Specifically, Fick's second law equation 1 describes the change in concentration at a specific point over time. The change over time in the composition within the element is obtained by the sum of the fluxes going in and out.

$$\frac{\partial \phi}{\partial t} = \nabla \cdot \left( D \nabla \phi \right) \qquad (1)$$

Where $\phi$ is the drug molecule concentration, $D$ is the diffusion coefficient, and $\vec{\nabla}$ is the differential operator $\left(\frac{\partial}{\partial x}+\frac{\partial}{\partial y}+\frac{\partial}{\partial z}\right)$. Equation 1 can be expressed in terms of *J,* the species flux, equation (2).

$$\frac{\partial \phi}{\partial t} = -\nabla \vec{J} \qquad (2)$$

$$\text{Where } \vec{J} = D\nabla\phi \qquad (3)$$

The change in concentration over time for a specified volume $\Omega$ is obtained by integrating equation 3 for the entire volume $\Omega$.

$$\iiint_{\Omega}\left(\frac{\partial \phi}{\partial t}+\vec{\nabla}\cdot\vec{J}\right)d\Omega \qquad (4)$$

The integration is performed using the divergence theorem equation 4 where $\vec{n}$ is the unit normal vector perpendicular to the surface $s$.

$$\iiint_{\Omega}\frac{\partial \phi}{\partial t}d\Omega + \oiint\left(\vec{J}_j\vec{n}\right)ds \qquad (5)$$

The surface integral can be applied to a volume element and expressed as a summation of the flux through each one of the faces $j$ of the volume element $i$.

$$\frac{\partial \phi_i}{\partial t}\Delta\Omega_i = \sum_{j=1}^{N_i}\vec{J}_{ij}\cdot\vec{n}_{ij}\Delta S_{ij} \qquad (6)$$

*1.2.2 Diffusion Coefficients in Biological Systems*

In dilute solutions, diffusion is caused by thermal energy derived from the collusion between solute molecules. The flow of solutes is slowed by the drag of the medium where the flow takes place[10]. The relation between the thermal energy and the drag of the medium is described by the diffusion coefficient. The diffusion coefficient is the most important parameter when describing diffusion in any medium. For diffusion of a molecule in a liquid, the Stokes-Einstein relation equation (7) takes into

consideration the shape and size of the molecule being diffused, as well as the viscosity of the liquid.

$$D_0 = \frac{k_B T}{6\pi\mu R_h} \quad \text{Stokes-Einstein Relation} \quad (7)$$

Where $k_B$ B is Boltzmann's constant, $k_B$ = 1.38x10^23 J/degrees, $T$ is the temperature in Kelvin, $\mu$ is the solvent viscosity, and $R_h$ is the hydrodynamic radius of the diffused molecule. Diffusion of molecules in drug delivery systems does not always take place in a liquid; hydrogels are commonly used for the delivery of drug agents. The diffusion coefficient of a gel can be approximated using the Carman-Kozeny model, which is a function of pore size ( $a$), and porosity ( $\varepsilon$). The model treats the gel as an array of cylinders randomly oriented in three dimensions characterized by the geometric factor $k$ [11].Carman-Kozeny model (equation 12) estimates the diffusion ratio between a gel and a solvent.

$$K = \frac{\varepsilon a^2}{4k} \quad (8)$$

$$k = (2k_{\perp} + k_{\parallel}) \quad (9)$$

$$k_{\parallel} = \frac{2\varepsilon^3}{(1-\varepsilon)\left[2\ln\left(\frac{1}{1-\varepsilon}\right) - 3 + 4(1-\varepsilon) - (1-\varepsilon^2)\right]} \quad (10)$$

$$k_{\perp} = \frac{2\varepsilon^3}{(1-\varepsilon)\left[2\ln\left(\frac{1}{1-\varepsilon}\right) - \frac{1-(1-\varepsilon^2)}{1+(1-\varepsilon^2)}\right]} \quad (11)$$

Equations 9-11 give the geometric factor for cylinders that are randomly distributed in three dimensions. Equations 10 and 11 give a factor of distribution for cylinders that are parallel and perpendicular to the flow, respectively. Equation 8 relates the permeability $K$, pore size, porosity, and the geometric factor. The effective diffusion of the gel can be obtained when the diffusion coefficient of the solvent is multiplied

with the diffusion ratio expressed in equation 12.

$$\frac{D}{D_0} = \frac{\alpha}{\left\{1 + \left(\frac{R_h^2}{k}\right) + \frac{1}{9}\left(\frac{R_h^2}{k}\right)\right\}} \quad \text{Carman-Kozeny model} \quad (12)$$

*1.2.3 Polymer Degradation*

Biodegradable polymers have gained importance for their applications in drug delivery. Drug molecules can be incorporated into the polymer's matrix and the drug release kinetics are controlled by drug diffusion, matrix swelling and matrix erosion [12]. The rate at which the drug is released depends on the degradation that is a result of the functional groups that make up the polymer [13]. For example, Poly (lactide-co-glycolide) (PLGA), the most commonly used FDA approved polymer for drug delivery systems, is composed of lactic and glycolic acid monomers as functional groups [6].

PLGA hydrolysis takes place in the ester bond, yielding functional groups that are cleared by the Krebs cycle. The rate of PLGA hydrolysis depends on the ratio of lactic and glycolic acid, because glycolic acid is more hydrophilic than lactic acid, thus increasing the hydrolysis rate [14, 15]. The ester carbon is subject to nucleophilic attack by water, and hydrolysis proceeds via a tetrahedral intermediate, yields a primary alcohol and a carboxylic acid shown in figure 1.1. The accumulation of carboxylic acid then leads to autocatalysis of hydrolysis [6, 12].

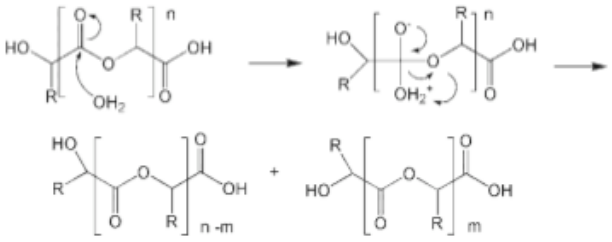


Figure 1.1 PLGA ester hydrolysis mechanism. R represents CH3 for lactide. The resulting primary alcohol can take a proton from the carboxylic acid during the chain cleavage. The protonation and deprotonation of the alcohol are facilitated by water [6].

*1.2.4 Modeling of Biodegradable Polymers*

Mathematical analysis of drug delivery vehicles has extended the understanding of how polymers' properties affect drug release[16]. Some current studies focus on either bulk or surface erosion behavior and assume that the drug release from the erodible system is proportional to its degradation [13]. Surface eroding is based on the assumption that the release takes place on the surface of the polymer and that the outer shape deteriorates as the polymer degrades [16]. Bulk eroding assumes that water penetrates into the matrix and that random degradation of the polymer occurs as a whole and not only on the surface [13, 17, 18].

The release kinetics of the system can be described using a first order release equation, taking into consideration the initial loading of the drug. However, this kind of model does not take into account the mechanism by which the drug is released. Korsmeyer and Peppas et al derived a simple model also known as Peppas equation shown in equation 13 that took into consideration the release from the surface of a polymer [19].

$$\frac{M_t}{M_\infty} = Kt^n \qquad \text{Peppas Equation} \quad (13)$$

Where K is geometry factor, t is the time, and n is a number that characterize the different release mechanisms of the polymer, table 1[20] summarizes the values of n factor. The result of the model is the accumulation of drug over time.

Table 1.1 Interpretation of diffusional release mechanism for a sphere

| Release Exponent (n) | Mechanism | Rate as a Function of Time |
|---|---|---|
| .43 | Fickian Diffusion | t^.43 |
| .43< n<.85 | Anomalous Transport | t^1-n |
| .85 | Polymer swelling | T^.85 |

## 1.3 Modeling Physical Phenomena

Mechanistic models take into consideration physical laws such as: diffusion, dissolution, and polymer degradation; they describe the mechanism by which drug release takes place. One of the advantages of using this approach for the implementation of a model is that it does not assume that the system is a “black box”; it actually takes into account all the phenomena involved in drug release and delivery. The aim of a mechanistic model is the determination of quantities that cannot be measured, but by the means of simulations that can be altered and the effect of such parameters could be understood. The modification of diffusion coefficients in a diffusion model is an example of simulation. [21-23]. Based on the real phenomena described by the model, an analytical solution can be derived if the model is simple; otherwise a numerical solution may be required. One of the drawbacks of mechanistic models is that they can get extremely complex, making them computationally expensive [17]. In order to find a numerical solution using mathematical techniques, such as the finite element analysis and the finite difference element method, are utilized.

Finite element method and finite difference method are two of the most common numerical solution approximation techniques for the solution of differential equations. Finite difference method is used to solve differential equations that have initial boundary conditions that change over distance. In contrast, finite element analysis (FEA) is based on initial value conditions that change over time. FEA has been used for the approximation of solutions for diffusion equations. Due to the nature of the equations utilized in this study and the initial conditions, FEA was determined to be more suitable for the approximations of the equations that describe the physical phenomena discussed in the previous section.

### *1.3.1 Finite Element Analysis Basic Concept*

The division of a complex problem into individual compartments, that are well understood, is a technique that scientists, engineers, and even economists utilize [24]. Finite element analysis method (FEA) is a powerful tool to approximate solutions for problems with complex domains and boundary

conditions. The concept was introduced by Turner et al (1956), and since has become one of the preferred methods for the modeling of physical phenomenon in a variety of disciplines[8].

The basic idea behind this method is that physical phenomena take place in a continuous matter. For instance a solid or a liquid, in order to completely describe it, an infinite number of points have to be taking in consideration[8]. Finite element method divides the domain, where the physical phenomenon is taking place, into smaller subdomains that keep the properties of the original[8, 25]. By solving each subdomain individually, the solution for the system as a whole can be approximated.

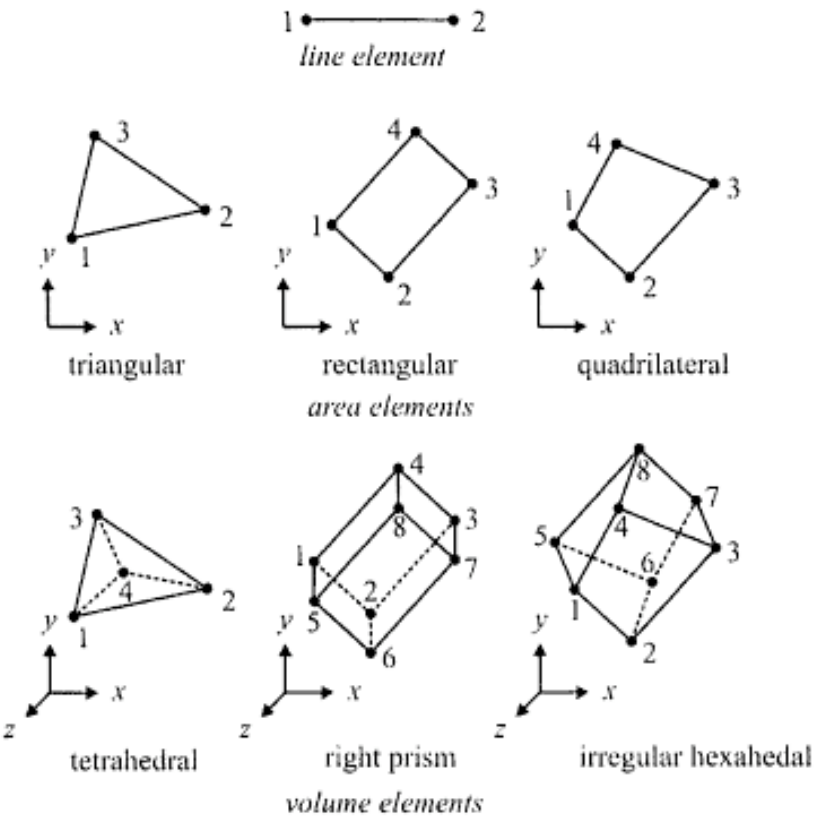


Figure 1.2 Description of characteristic line, area, and volume elements with the corresponding node numbers [8].

One of the main advantages of FEA over other methods is the adaptation to irregular domain shapes, allowing the analysis of a broad number of problems involving initial value and Eigen value problems in many disciplines [8]. There is a methodology for the application of FEA to a specific

problem. The first step is the breakdown of the main domain for the problem. This is achieved by creating a mesh in which the elements do not cross boundaries and reside in only one of the domains, since the problem can contain several domains with different properties. Next, the interpolation equations have to be selected; this step depends on the kind of problem that is being solved, for example differential equations are involved in heat transfer. Once the equations are set up, matrices have to be assembled for each one of the subdomains and a global matrix is formed with all the subdomain matrices. Once the global matrix is assembled, the boundary conditions are applied. This is a critical step since if the boundary conditions are not chosen correctly; the model might not approximate the right solution. Finally the solution for the equations is approximated.

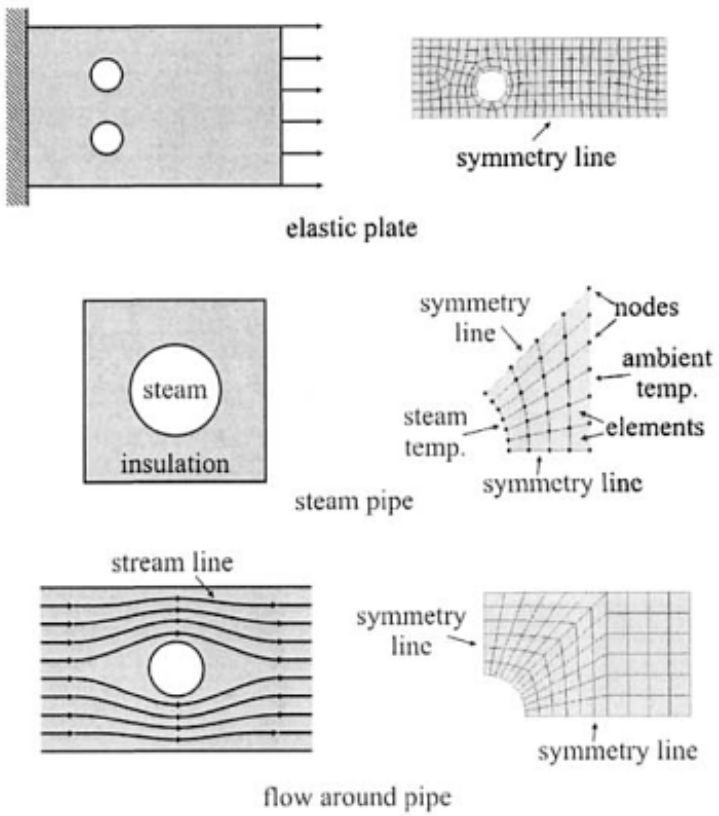


Figure 1.3 FEA representation of practical engineering problems. Showing the breakdown of the domain into subdomains containing nodes, boundary conditions and subdomain elements.

## 1.4 Current Approaches

Advances in computer technology have led to an increase in the mathematical modeling of drug delivery systems. The development of mathematical model has been limited to biodegradable polymer release and release from polymer matrixes[26, 27]. There are only a few publications describing the kinetics of drug release and the diffusion into an external medium. Zhou et al implemented a multiparticulate system made up of microcapsules that released into a finite volume, and the effects of the accumulation of drug was observed in the release rate [28]. The results of this study provided an accurate prediction of the release kinetics for this kind of system when parameters such as the initial concentration and the volume of the medium are modified.

Batycky et al. developed a bulk-eroding model for the release of macromolecules from 50/50 PLGA microspheres. The model takes into consideration the presence of an initial burst followed by diffusion via interconnected pores. This model was the base for more current models like the one developed by Lao et al. that takes into consideration a three-step sequence [29, 30]:

- Penetration of solvent into the matrix.
- The creation of a free volume within the matrix for drug dissolution “relaxation of the network”.
- Drug removal to the surrounding medium, usually by diffusion.

The release profile varies with respect to the properties of the polymer and the drugs being released. Specifically, a model for PLGA that takes into consideration all three steps and the partial fraction of drug release is summarized in Equation (14) [30].

$$\begin{aligned}\left\{\frac{M_t}{M_\infty}\right\} &= \phi_{b,PLGA}\left\{1-\exp(-k_{b,PlGA}t\right\} \\ &+\phi_{r,PLGA}\left\{\exp[k_{r,PLGA}(t-t_{b,PLGA})]-1\right\} \\ &+\phi_{d,PLGA}\left\{1-\sum_{n=0}^{\infty}\frac{8}{(2n+1)^2\pi^2}\exp\left(\frac{-D_{PLGA}(2n+1)^2\pi^2(t-t_{r,PLGA})}{4l^2}\right)\right\}\end{aligned} \quad (14)$$

Where $\left\{\frac{M_t}{M_\infty}\right\}$ is the total fraction of drug release from PLGA, and it is denoted as the sum of the initial burst, the relaxation of the network, and the diffusion to the surrounding medium. All the parameters are defined in table 1.2[30]. This kind of mechanistic model has proven accurate, but its complexity makes it hard to implement.

Table 1.2 Model parameters for Lao's PLGA drug release model.

| Parameter | Description |
|---|---|
| $\phi_{b,PLGA}$ | *Fraction of burst release from PLGA* |
| $k_{b,PLGA}$ | *Burst constant of PLGA* |
| $t$ | *Time* |
| $\phi_{r,PLGA}$ | *Fraction of burst release from PLGA* |
| $k_{r,PLGA}$ | *Degradation relaxation constant of PLGA* |
| $t_{b,PLGA}$ | *End of burst release for PLGA* |
| $\phi_{d,PLGA}$ | *Fraction of drug release through diffusion for PLGA* |
| $D_{PLGA}$ | *Drug diffusion coefficient for PLGA* |
| $l$ | *Half thickness* |

Models based on the diffusion in hydrogels have also been developed and have proven accurate. Charalamboulou et al. developed a model for diffusion in a multilaminate polymer matrix solved using a moving boundary, and finite element analysis model to approximate the solution [31].

## 1.5 Project Aims

Currently all the drug delivery computer models have been based on the drug release from an erodible polymer, or the diffusion of the drug through a polymer matrix. The purpose of this project is the development of a combined model that considers the drug release from an erodible polymer and its diffusion through the surrounding medium. The model is based on cylindrical scaffolds used in nerve guidance and angiogenesis. This will enable the prediction of the drug concentration generated from drug release. Specifically the aims of this project are:

1. Develop a drug diffusion model for hydrogels using the Fick's second law of diffusion and finite element analysis.
2. Implement a multimedium drug delivery system model based on cylindrical scaffolds with and without microchannels.
3. Incorporate release from loaded PLGA microparticles into the model.

CHAPTER 2

# DESIGN AND IMPLEMENTATION OF 3D MULTI-MEDIUM DRUG RELEASE COMPUTER MODEL

## 2.1 Modeling Details

The development of the model is in steps, described by the specific aims. Each specific aim is the basis for the next step, when putting the end results of each specific aim shown in figure 2.1.The end result is a model that estimates the drug concentration in space and time within the volume of the system modeled. The model is based on two configurations of a scaffold utilized for nerve regeneration and angiogenesis, in which a concentration of growth factors had to be achieved within the lumens of the two devices.

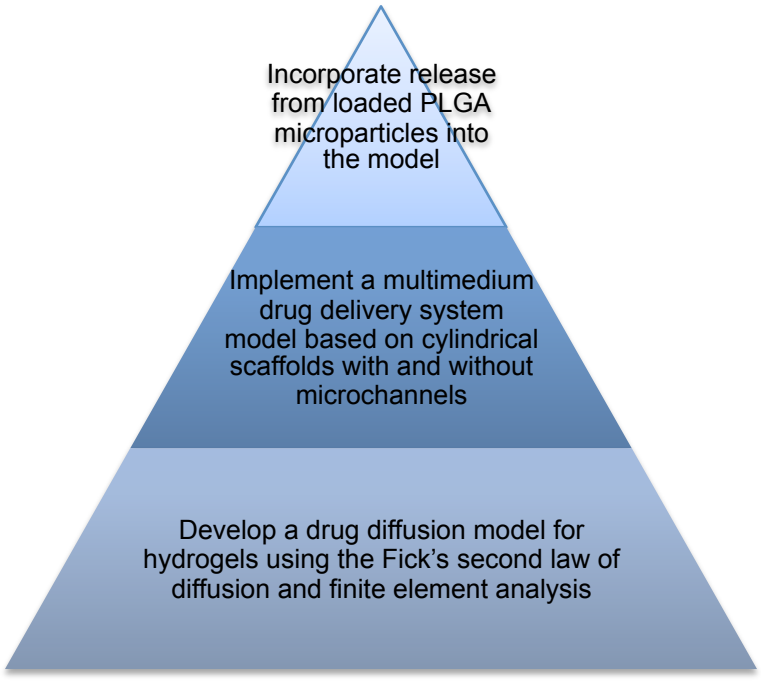


Figure 2.1 Organization of specific aims for model development.

The multi-medium drug release model is based on Fick's second law of diffusion, which describes how diffusion affects the concentration field with respect to time. The main parameter affecting diffusion is the diffusion coefficient. That is calculated using the Carman-Kozeny model, taking into consideration the pore size and the porosity of the hydrogels utilized in the drug delivery system. In one of the conformations, 50/50 PLGA microparticles are modeled using a modified Krosmeyer-Peppas model. The specific parameters calculated and a detailed sequence of the calculation for the diffusion model for hydrogels is summarized in figure 2.2.

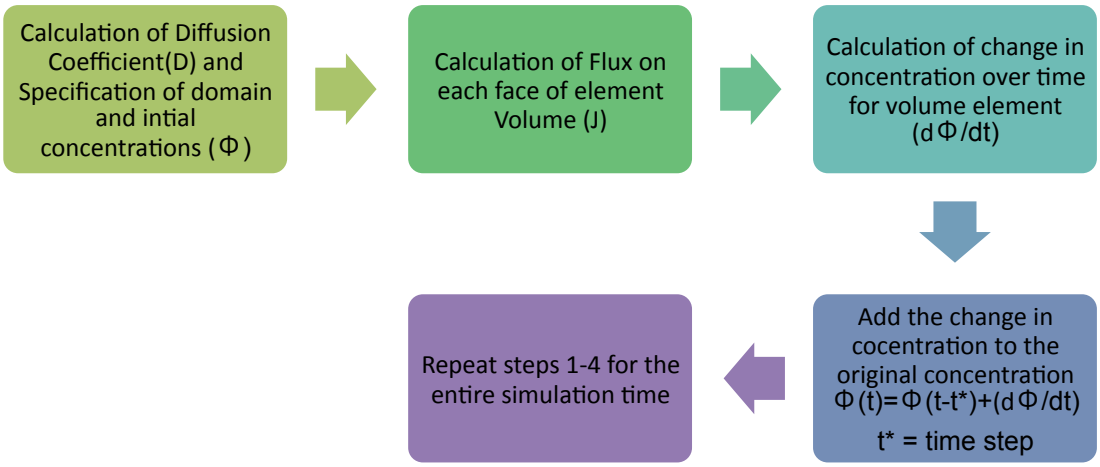


Figure 2.2 Sequence of calculations and specific parameters for the diffusion in hydrogels.

The summary in figure 2.2 specifies the steps and specific parameters for the calculation of the diffusion in the hydrogel medium specified in specific aim 1. After this procedure was implemented for a medium composed of a specific hydrogel, the geometry of the drug delivery device was implemented and different gel mediums were considered; this step is part of specific aim 2. Finally, the incorporation of loaded PLGA microparticles was incorporated into the model (specific aim 3). The sequence of calculations and specific parameters are summarized in figure 2.3.

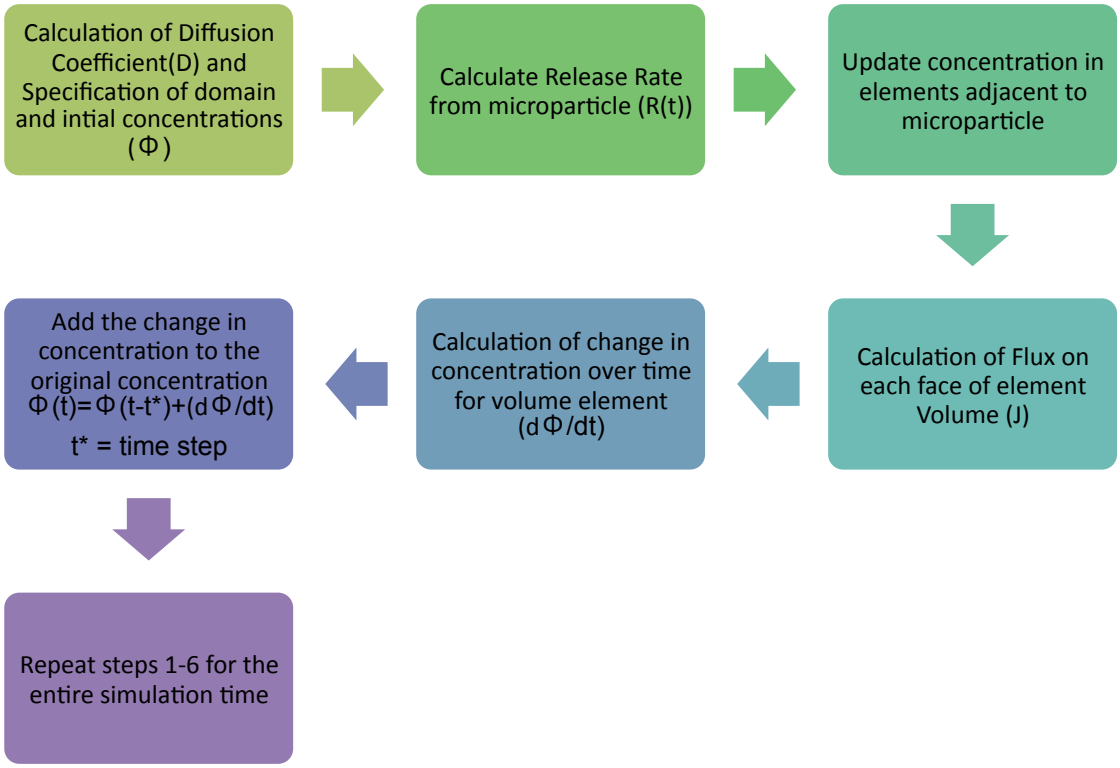


Figure 2.3 Sequence of calculations and specific parameters for the diffusion in hydrogels with the incorporation of PLGA microparticles.

## 2.2 Calculation of Diffusion Coefficients

Diffusion coefficients represent the hindering of a medium for the motion of macromolecules, in this case the motion of drug molecules. As mentioned in the introduction, the Brinkman (or effective medium) model and Stokes-Einstein relation can be utilized for the calculation of the diffusion coefficient of a molecule in a hydrogel, in terms of the molecule hydrodynamic radius of the diffused molecule, and the porosity of the porous medium, in this case the hydrogel [32, 33].

Two different gels were considered for the implementation of the model. Agarose, a polysaccharide obtained from agar that is used for a variety of life science applications, and collagen, a fibrous extracellular matrix protein commonly used in drug delivery systems. In order to obtain the diffusion coefficient of a drug molecule in the different gels, the Brinkman (or effective medium) model in

combination with the Carman-Kozeny model as described in the introduction, was utilized. Unfortunately, the model calculates the ratio of a molecule's diffusion coefficient in the medium and solution [34].

The gel diffusion coefficient was calculated by multiplying the ratio obtained from the effective medium model with the diffusion of the molecule in the solvent (water), calculated using the Stokes-Einstein relation. The calculation of diffusion coefficients in the solvent were calculated using MATLAB 7.9 R2009B (The MathWorks Inc.) and were based on values for the viscosity of water of .89 mPas [35], at a temperature of 310 degrees Kelvin, for a range from 1 to 100 nm for the hydrodynamic radius. The results are summarized in figure 2.4.

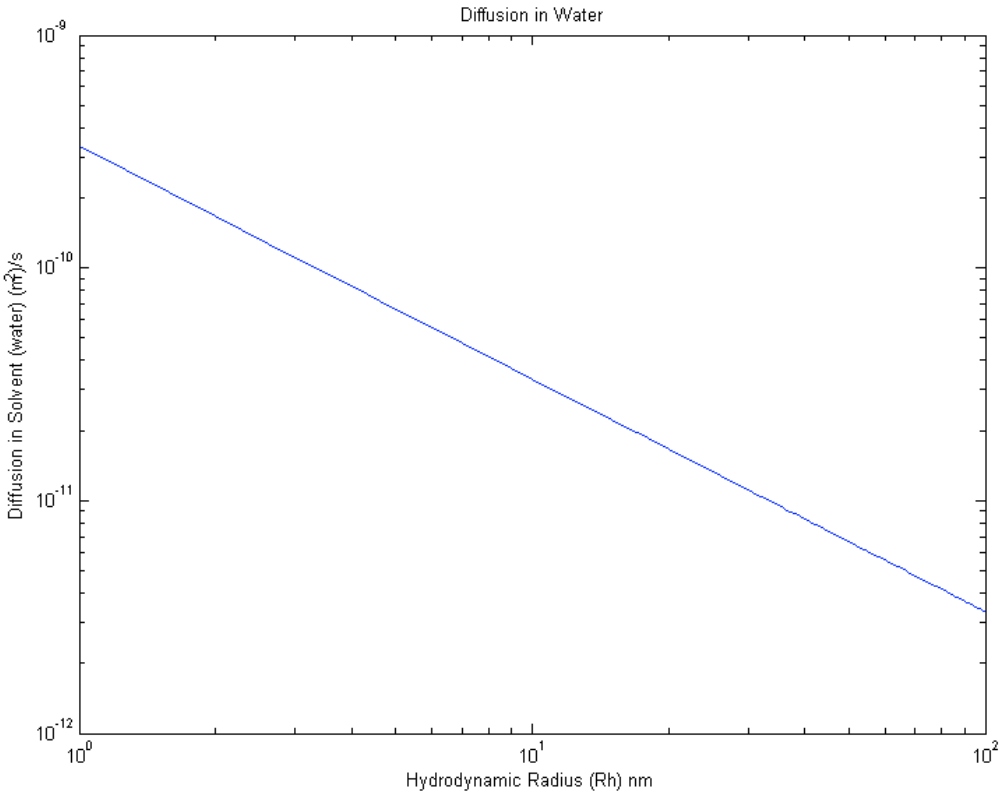


Figure 2.4 Relationship of hydrodynamic radius and diffusion coefficient. The increase in the hydrodynamic radius of a molecule decreases the diffusion coefficient in water.

The next step in the calculation of the effective diffusion coefficient in the gels was the calculation of the ratio of the molecule diffusion coefficient for the medium and solution, using the Brinkman model.

The parameters used for this calculation are summarized in table 2.1. The effective diffusion in the gels was obtained by taking into consideration the diffusion in water as the solvent diffusion. The effective diffusion in the gel is shown in figure 2.5.

Table 2.1 Model parameters for effective medium model for Collagen .1 % and Agarose 1.5 %

| Parameter | Value | Source |
|---|---|---|
| Porosity (ε) (agarose 1.5%) | .805 | [36] |
| Pore Size (a) (agarose 1.5%) | 150 nm | [36] |
| Porosity (ε) (collagen .1%) | .890 | [34] |
| Pore Size (a) (collagen .1%) | 470 nm | [32, 34] |

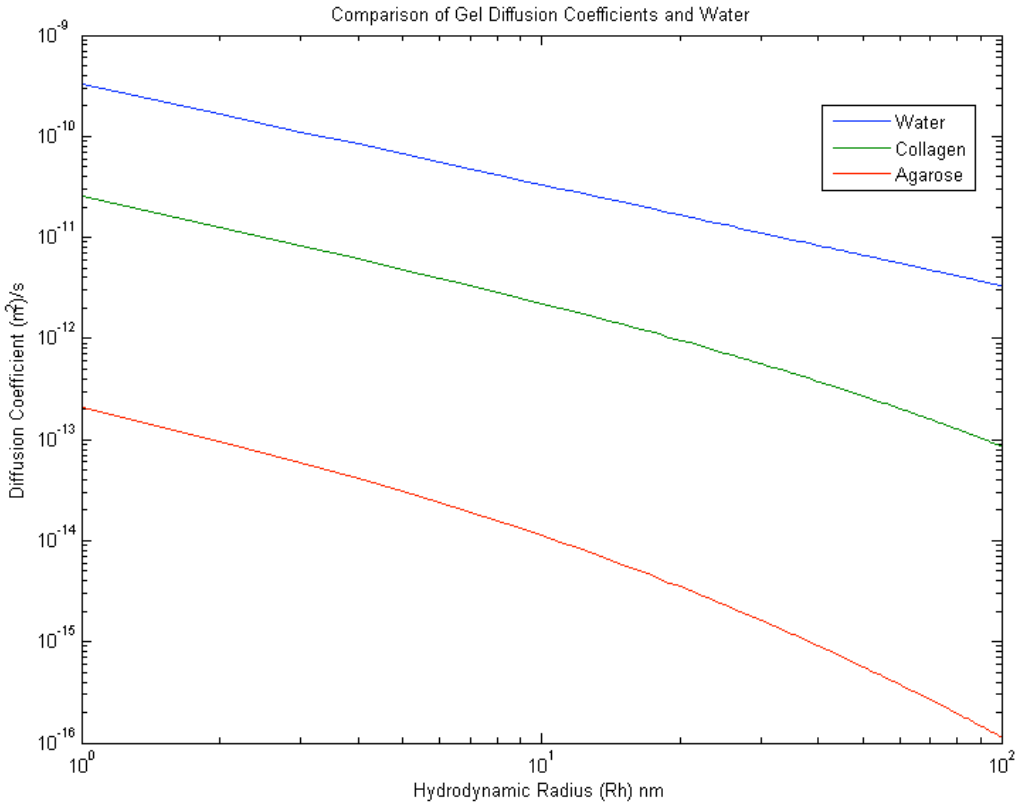


Figure 2.5 Relationship of hydrodynamic radius and diffusion coefficient in agarose, collagen, and water.

## 2.3 Calculation of Drug Release Kinetics from PLGA Microparticles

In order to incorporate the PLGA microparticles into the model, spheres representing PLGA loaded microparticles were uniformly distributed in the lumen of both devices using a random coordinate generator based on a normal distribution with a high standard deviation as shown by Huang et al.[37]. Once the spheres were set in place, their release profile was implemented using a modification of the Korsmeyer-Peppas Model which relates the exponential drug release with time. Korsmeyer Model takes into consideration the shape of the degradable polymer and the release mechanism, which can either be Fickian diffusion, anomalous transport, or case II transport (zero order release) [19, 38, 39]. A constant, K, represents the geometry of the release polymer, and an exponential, n, describes the release mechanism. Using a value of K=.37 for the constant K and an n=.25, the Korsmeyer Peppas formula was implemented for a period of 30 days (figure 2.6).

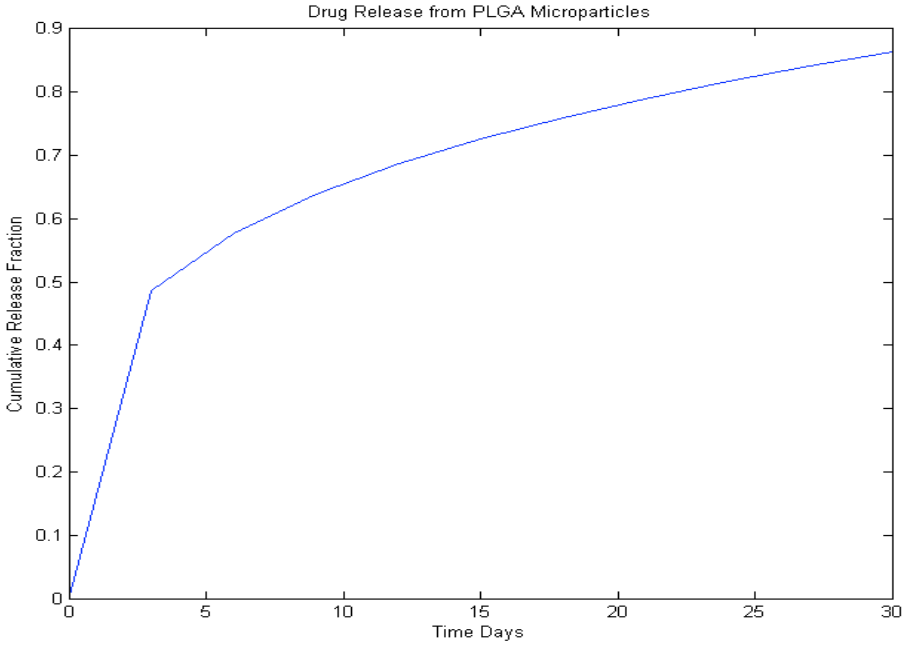


Figure 2.6 Fraction drug release derived from Korsmeyer-Peppas Equation.

The result is the release profile for the cumulative release of drug over time. However, the microspheres in the model are modeled as solute sources, and implementation of the formula yields the cumulative release, not the release rate at a specific time. In order to obtain the release rate as a function of time, the derivative of Korsmeyer equation was calculated, finding the values at zero yielded an undefined solution. A forward differentiation calculation was added to the code, calculating the release rate over time (figure 2.7).

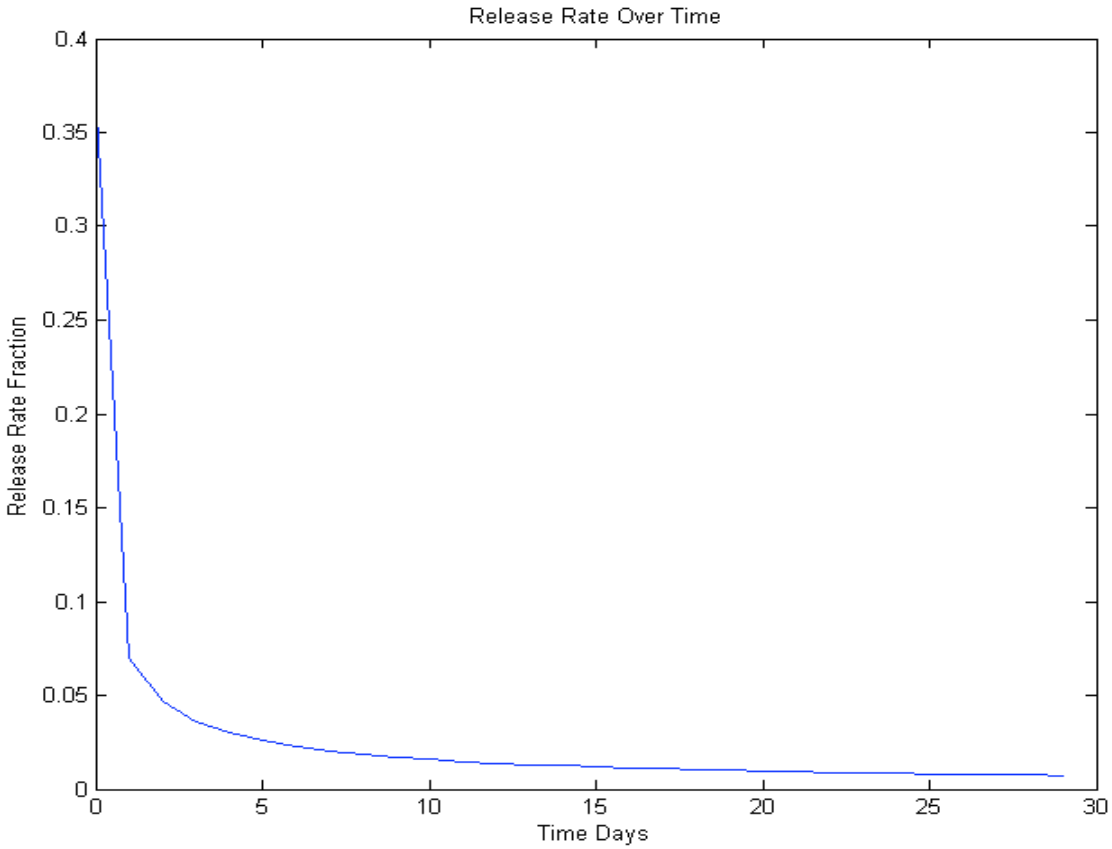


Figure 2.7 Calculated release rate over time.

## 2.4 Model Geometry

The geometry of the configuration of the model is based on a nerve guide used in regenerative sieve electrodes, and a multichannel scaffold filled with a collagen matrix used in nerve regeneration and angiogenesis for engineered organs [40]. The first configuration consists of a hollow Crosslinked Urethane Doped Polyester Elastomer (CUPE) tube (Micro-Renathane®, Braintree Scientific, Inc; OD 3 mm, ID 1.75 mm, and7 mm in length) filled with collagen I/II (0.3% Chemicon Tamacula, CA, USA). The geometry was implemented in COMSOL Multiphysics CAD environment using a solid cylinder with a diameter of 3mm and a length of 10mm intersected with another cylinder with the radius of 1.75 mm and 10mm in length. Actual picture and model geometry are shown in figure 2.8.

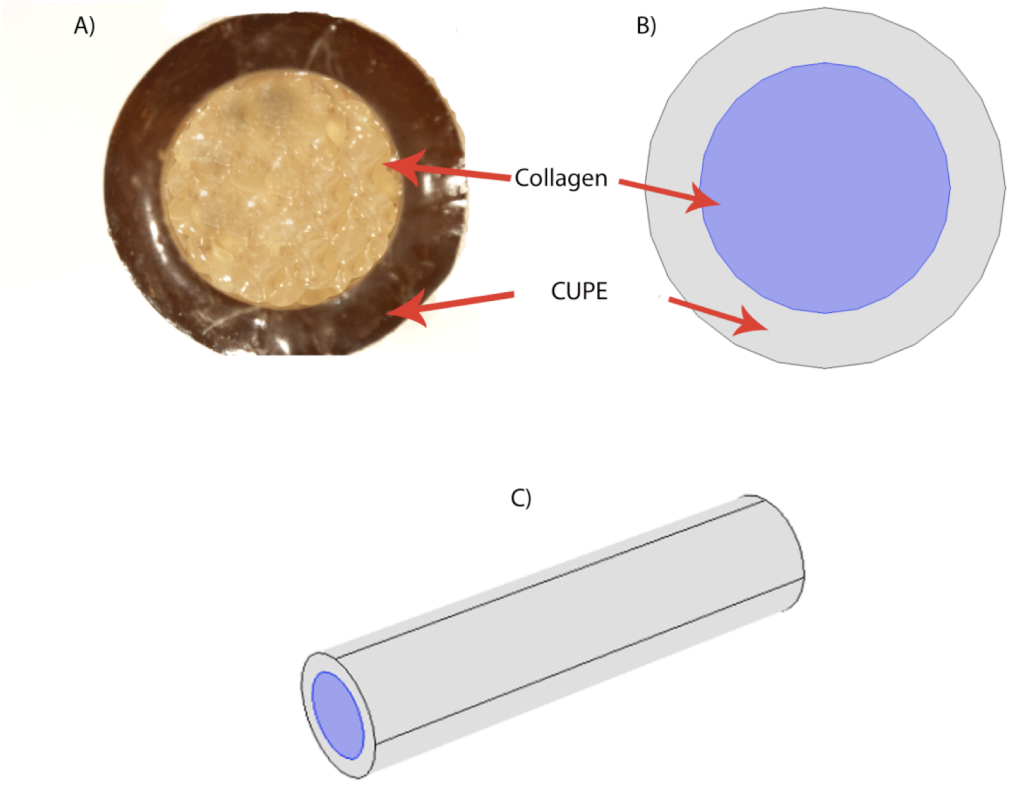


Figure 2.8 Single channel configuration of drug delivery system. A) Image of single channel nerve guide for sieve electrodes. B) Top view of model geometry. C) Isometric view of the model.

The second configuration consists of a multiluminal tube containing seven microchannels of 250 micrometers (µm), and a central channel of 350 µm in diameter. A similar geometry of the device was previously implemented by Tansey et al and refered to as a biosinthetic nerve implant (BNI) [40]. In the design described by Tansey et al, the outer tube is a Micro-Renathane® tube (Braintree Scientific, Inc; OD 3 mm, ID 1.75 mm, and length of 12 mm) made out of CUPE, and the matrix consists of agarose microchannels filled with collagen. The model geometry was created using COMSOL Multiphysics Modeling and Engineering Simulation Software Version 4.0 CAD environment. The dimension of the geometries was kept as described in the publications in order to make the simulations more accurate. During the creation of the geometries, the different mediums were taken into consideration, to avoid mesh elements in two boundaries as explained in the finite elements analysis section of the introduction. Figure 2.9 shows the implementation of the geometries for the two conformations of the drug delivery system model.

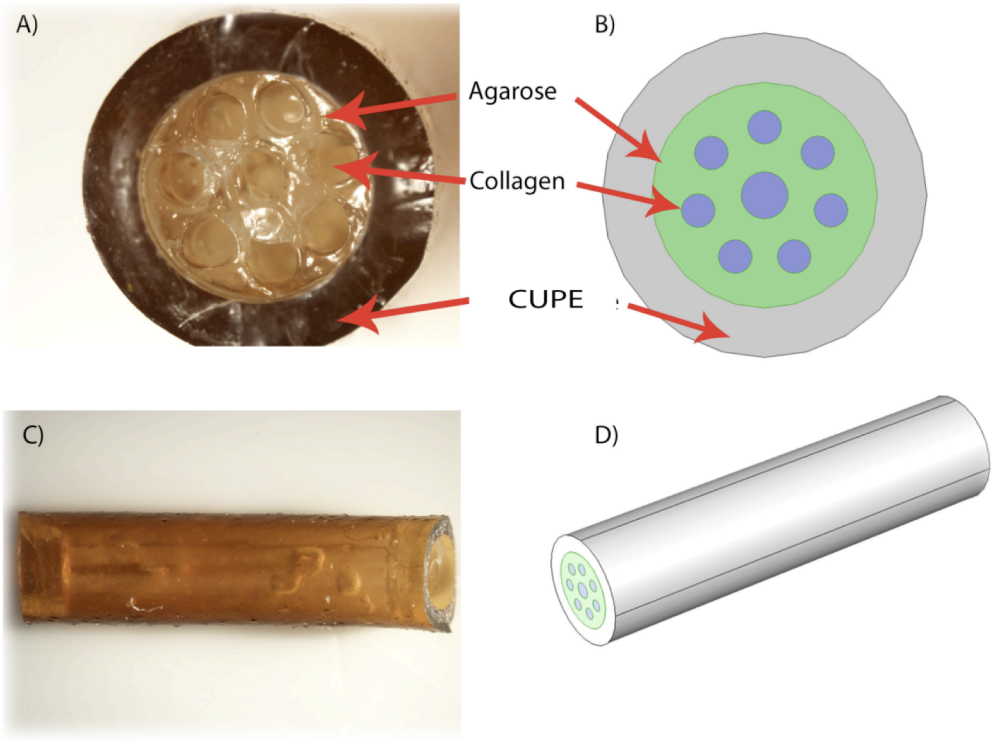


Figure 2.9 Multiluminal configuration of drug delivery system. A) Image of multiluminal biosynthetic nerve implants (BNI). B) Top view of model geometry. C) Isometric view of the model.

Dawood implemented a similar device as a drug delivery system to promote angiogenesis in vitro, utilizing loaded PLGA microparticles with vascular endothelium growth factor (VEGF) [41]. A model depicting this configuration was implemented. The development of the geometry for the model, including polymer microparticles, was generated using a random three-dimensional coordinate generator for the locations of the microparticles. Limits for the coordinate generator were set for the boundaries of the cylinder with the dimensions of the microchannels in the multiluminal arrangement and the inner lumen in the single channel arrangement. The coordinates were calculated in MATLAB 7.9 R2009B (The MathWorks Inc.) using a pseudorandom value generator. The pseudorandom value generator draws its values from a normal distribution for the interval set by established limits. Once the coordinates were obtained, spheres of 5 μm in diameter were placed at each location. A total of 63 spheres were placed in the lumen of the single channel arrangement, and 55 in the microchannel of the multiluminal arrangement. Configurations for the single and multiluminal devices with microparticles are shown in figures 2.10 and 2.11, respectively.

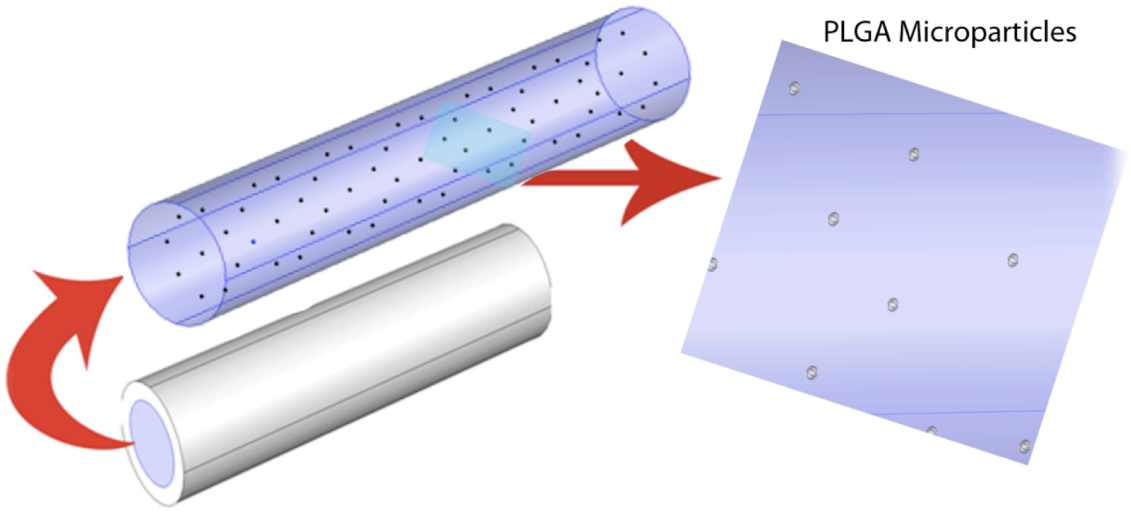


Figure 2.10 Single channel arrangement of drug delivery system filled with loaded PLGA microparticles.

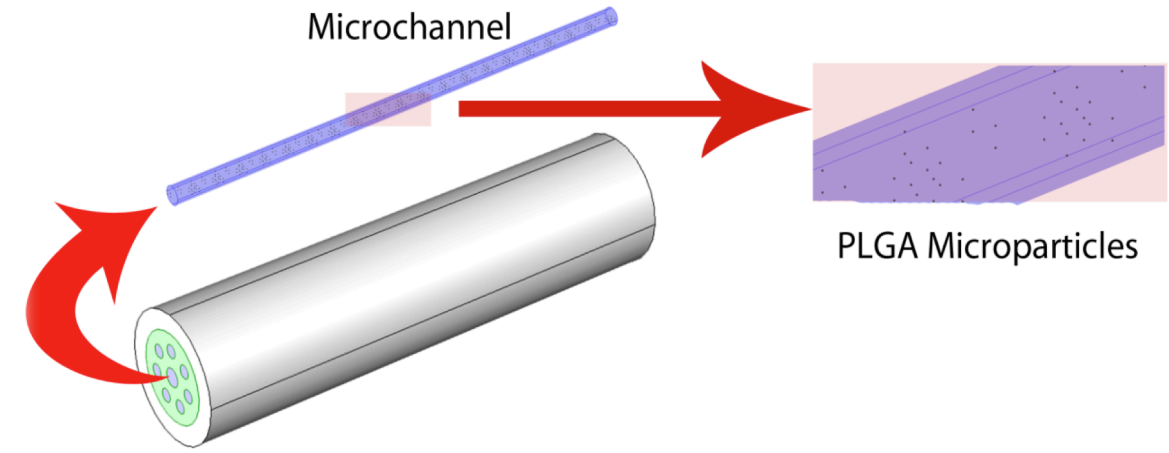


Figure 2.11 Multiluminal configuration of drug delivery system filled with loaded microparticles.

## 2.5 Mesh Generation

Mesh generation is fundamental for the implementation of an accurate model, since a misrepresentation of the geometry can affect the result of the calculations. The geometries created for each one of the models, were converted into a mesh using COMSOL Multiphysics Modeling and Engineering Simulation Software Version 4.0 meshing module using tetrahedral, triangular, and hexahedral mesh elements for the boundaries. The size was set to normal, which gave a maximum element size of 1000 μm, minimum of 180 μm, maximum element growth rate 1.5, and a curvature resolution of .6. The maximum growth rate of an element specifies an element cannot be bigger than its neighbor for more than a factor of 1.5. Since the model is three-dimensional, the mesh is composed of volume elements.

After running the automated mesh generator, the mesh was inspected for any discontinuities and inverted mesh elements that usually appear near the edges and small elements. The identification of the problems is critical, since a discontinuity stops the program. If a discontinuity was found, it was fixed manually by connecting the mesh nodes. The implementation of the single channel only produced an inverted mesh element at the location (0, 0, 1E-5). Figure 2.12 shows the final implementation of the mesh for the single channel delivery system.

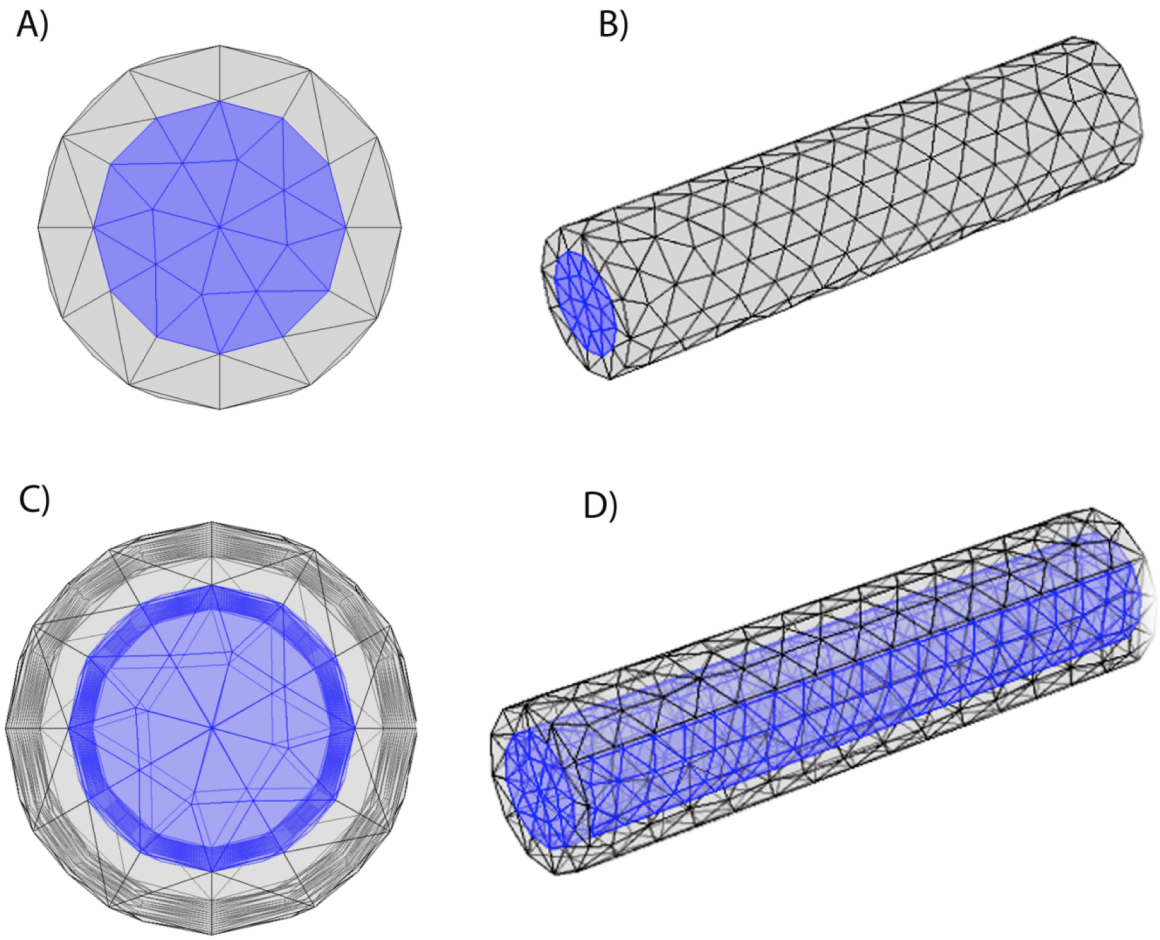


Figure 2.12 Mesh of single channel drug delivery. A) Top view of the mesh boundary elements. B) Isometric view of surface mesh elements. C) Transparent top view showing internal arrangement of the mesh elements and their distribution in the internal boundaries. D) Isometric view of the internal mesh elements and their domains.

The mesh of the single channel drug delivery system is made up of 2957 tetrahedral and 1104 triangular elements for a mesh volume of 4.443E10 μm^3. The mesh is also divided into two domains that represent the two different materials depicted in the model. The shaded blue volume represents the lumen filled with collagen, and the gray outer volume represents the CUPE tube.

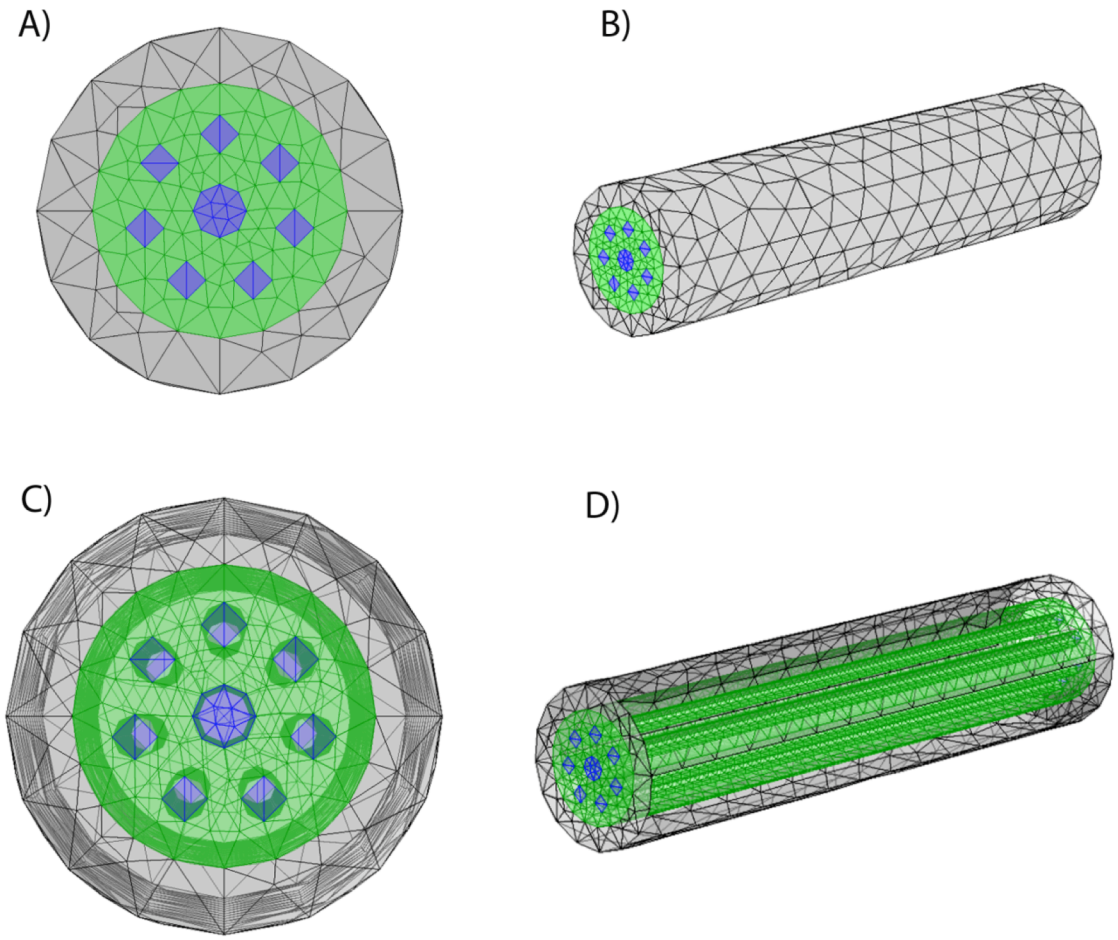


Figure 2.13 Mesh of multiluminal configuration of drug delivery system. A) Top view of the mesh boundary elements. B) Isometric view of surface mesh elements. C) Transparent top view showing internal arrangement of the mesh elements and their distribution in the internal boundaries. D) Isometric view of the internal mesh elements and their domains.

The implementation of the mesh for the multiluminal arrangement of the delivery system contained a total of 43146 tetrahedral and 9756 triangular elements for a volume of 4.449E10 μm^3. The mesh elements were divided into three domains: the outer volume shown in gray representing the CUPE, the green domain representing the agarose region of the device, and the blue domain representing the collagen region.

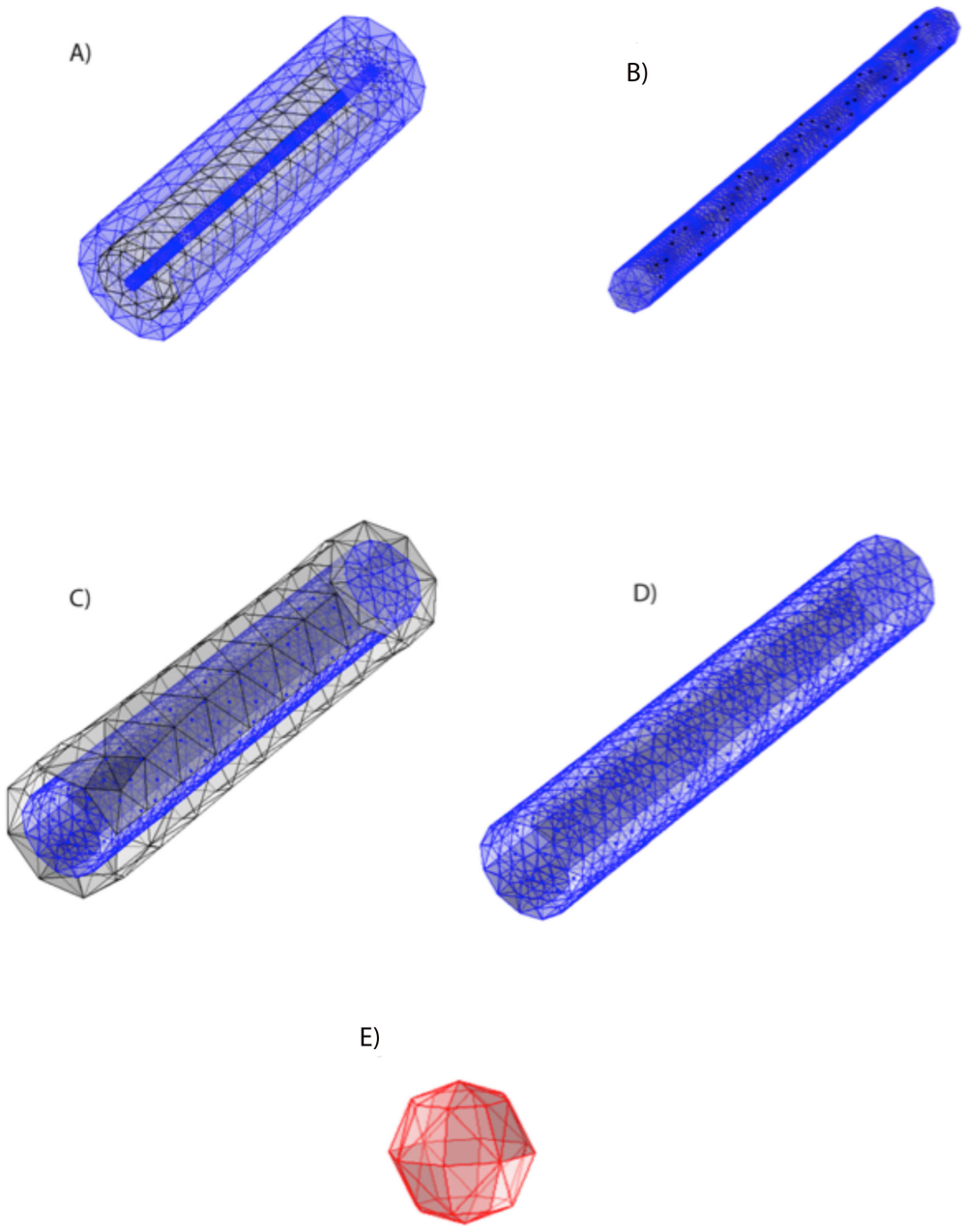


Figure 2.14 Mesh of single channel and microchannel arrangement with suspended microparticles. A) Isometric transparent view of multiluminal arrangement. B) Separated mesh of microchannel. C) Isometric view of single channel. D) Isometric view of internal mesh with microspheres of single channel. E) Meshing of microsphere.

Due to the large number of mesh elements for the implementation of the mesh including microparticles, the number of elements in the mesh size had to be coarser than normal. The microchannel contains 116024 tetrahedral, 4800 triangular and 1325 edge elements.

## 2.6 Model Validation

In order to verify that the finite element diffusion model described in specific aim 1, the solutions obtained for the model was compared using simple matrix system for a sphere in perfect sink conditions exact solutions described in literature [42]. The release of a drug from a swollen hydrogel is described by Fick's law as described in previous sections. The solution for the diffusion equations can be calculated using the respective appropriate geometry and boundary conditions. The result from the diffusion equation yields the concentration of solute at a specific point in time. By integrating over the geometry volume the release fraction can be calculated. The solutions for specific geometries are reported in literature [42].

The exact solution for a long cylinder of radius  with uniform concentration below the solubility limit of the drug, with the surface kept at a constant concentration, the mass of drug diffused at time t divided by the diffused drug at infinity (release fraction) is

$$\frac{M_t}{M_\infty} = 1 - \sum_{n=1}^{\infty} \frac{4}{a^2 \alpha_n^2} \exp(-D\alpha_n^2 t) \qquad (15)$$

Where  are the positive roots of, the Bessel function of the first kind of order zero.

The diffusion from a sphere of radius  under the same conditions can be obtained by:

$$\frac{M_t}{M_\infty} = 1 - \frac{6}{\pi^2} \sum_{n=1}^{\infty} \frac{1}{n^2} \exp(-\frac{Dn^2\pi^2 t}{a^2}) \qquad (16)$$

A three dimensional model for a sphere and a cylinder with a radius  under a finite volume of 1 liter was implemented using the developed model. The release profile was calculated and plotted for both geometries. Figure 2.15 shows the release profiles from the developed model and the exact solutions for both geometries. The calculated release profiles have a good agreement with the exact solutions with correlation coefficients of $R^2 = .995$ for the cylinder and $R^2 = .996$ for the sphere.

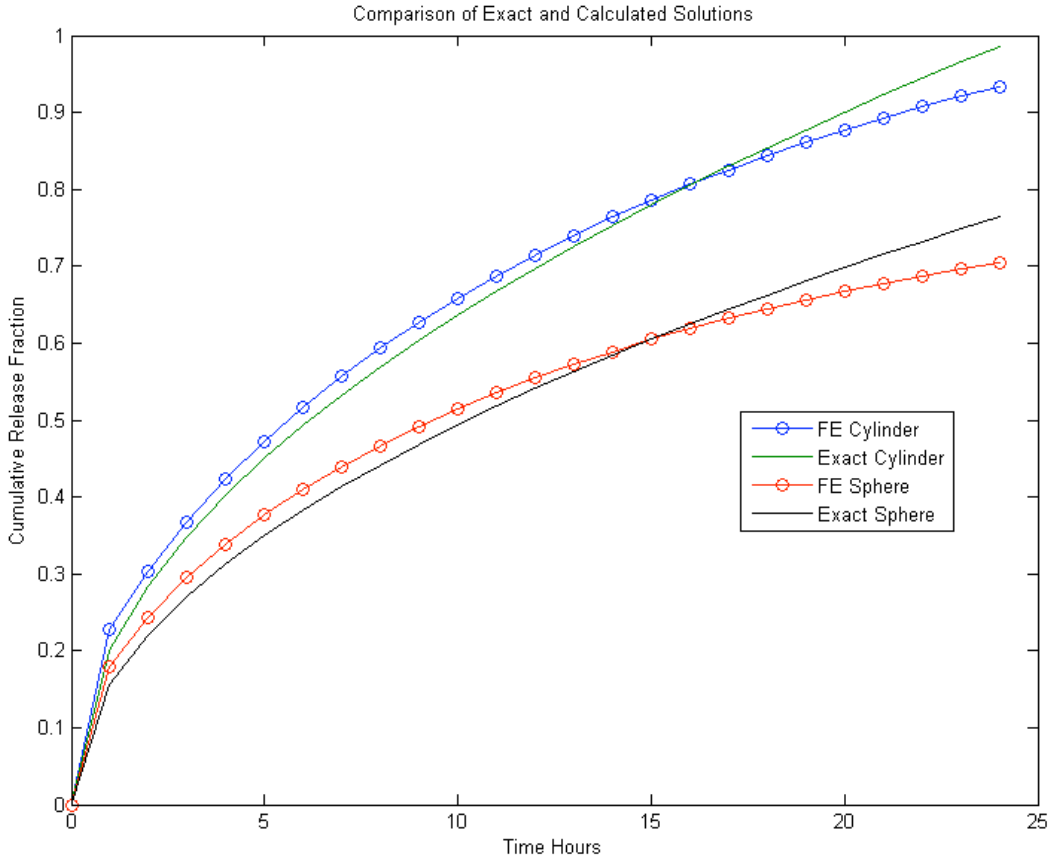


Figure 2.15 Release profiles for a sphere and a long cylinder with radius under perfect sink conditions and uniform concentration, calculated using the developed diffusion method (FE) and the exact solutions from literature.

The release profile from loaded PLGA microparticles was modeled using a modified version of Korsmeyer-Peppas equation for the release from a degradable polymer. Using data obtained from a release study performed using an ELISA kit for the release of loaded Pleiotrophin (PTN) loaded 50/50

PLGA microparticles. The predicted release profile obtained from the model developed was compared with the release profile measured with the ELISA kit. The release profiles are shown in figure 2.16 shows a good agreement of the predicted release with the measured release, a correlation coefficient of $R^2 = .995$ was calculated.

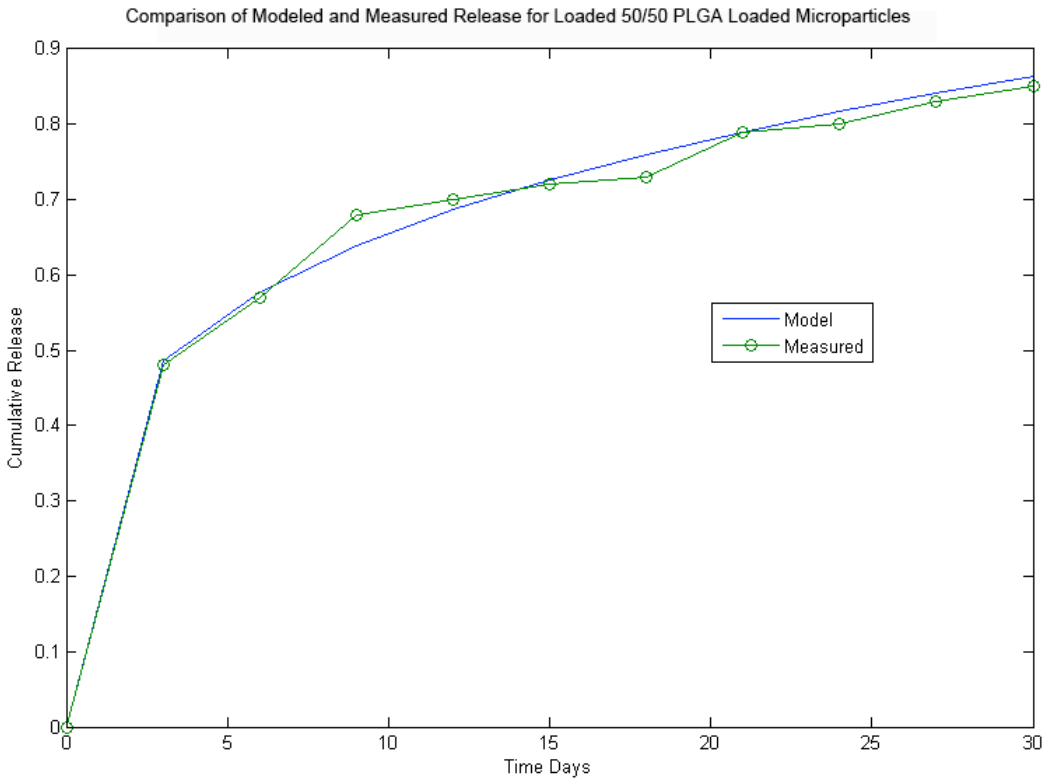


Figure 2.16 Comparison of predicted and measured release profile from PTN loaded 50/50 PLGA microparticles.

CHAPTER 3

# SIMULATION OF MULTIMEDIUM DRUG DELIVERY DEVICE

## 3.1 Simulation of Drug Diffusion Model for Hydrogels

### *3.1.1 Simulation Overview*

An agarose and a collagen cube of .1 cm side length were modeled with an initial uniform concentration of 100 mg/ml. The region consisted on a volume of .01 cm^3 located parallel to one of the sides of the cube and was modeled for 24 hrs with a molecule with a hydrodynamic radius of 40 nm (fig. 3.1).The diffusion coefficient was calculated to be 7.6 E -12 m^2/sec for collagen, and 2.31 E -14m^2/sec for agarose. The purpose of this block study is to determine the effect of the different hydrogels in the hindering of drug diffusion, and the determination of the time that the molecule will remain in the hydrogel. The boundary conditions were set to no flux for 5 of the faces and free flow for one of them, in order to direct the flow in that specific direction.

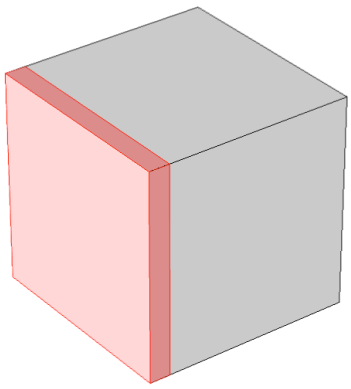

Figure 3.1 Boundary and initial conditions for cube study; shaded red area shows the initial concentration of solute, the rest of the faces shown in gray represent no flux boundary and the side opposite to the region of concentration has a free flow boundary.

The simulation code was implemented and first ran using COMSOL Multiphysics 4.0, further simulations were ran using MATLAB 7.9.0 r2009b with the generated code in COMSOL. To ensure the

reproducibility of the solution, the simulation was performed 5 times, each time the approximated solution was the same. Each simulation took 25.35 seconds to run using a 2.4 GHz Intel® Core™2 Quad processor computer.

### *3.1.2 Simulation Results*

The results of the simulation for the collagen block are summarized for the 24 hrs of the simulation with output times every 3 hours in figure 3.2.The diffusive flux of the solute is drawn as red arrows in the direction of the flux and proportional in size to the flux magnitude. The change in the concentration is shown as a color change; the values of the concentration color are shown in the color bar in the same figure. The diffusion in the cubes was observed to be uniform following the direction of the face with the free flow boundary condition. The average concentration over the initial loaded volume is monitored for the entire simulation time. The change in concentration over time is summarized in figure 3.4 along with the change in concentration for the agarose block.

For the agarose block simulation, the same time points were considered for the simulation. The results for the agarose diffusion model are summarized in figure 3.3. The red arrows show the diffusive flux direction and the size is proportional to the flux magnitude. The concentration is depicted as a color level shown in the colorbar in the same figure. It was observed that, as with the diffusion in collagen, the direction of the flux is towards the face with the free flow boundary condition, however, the diffusion was not as fast as in the collagen. In 24 hours, changes in the concentration were only observed near the loaded volume. The average concentration of the initial loaded volume is shown in figure 3.4 along with the average concentration of the same region for the collagen block.

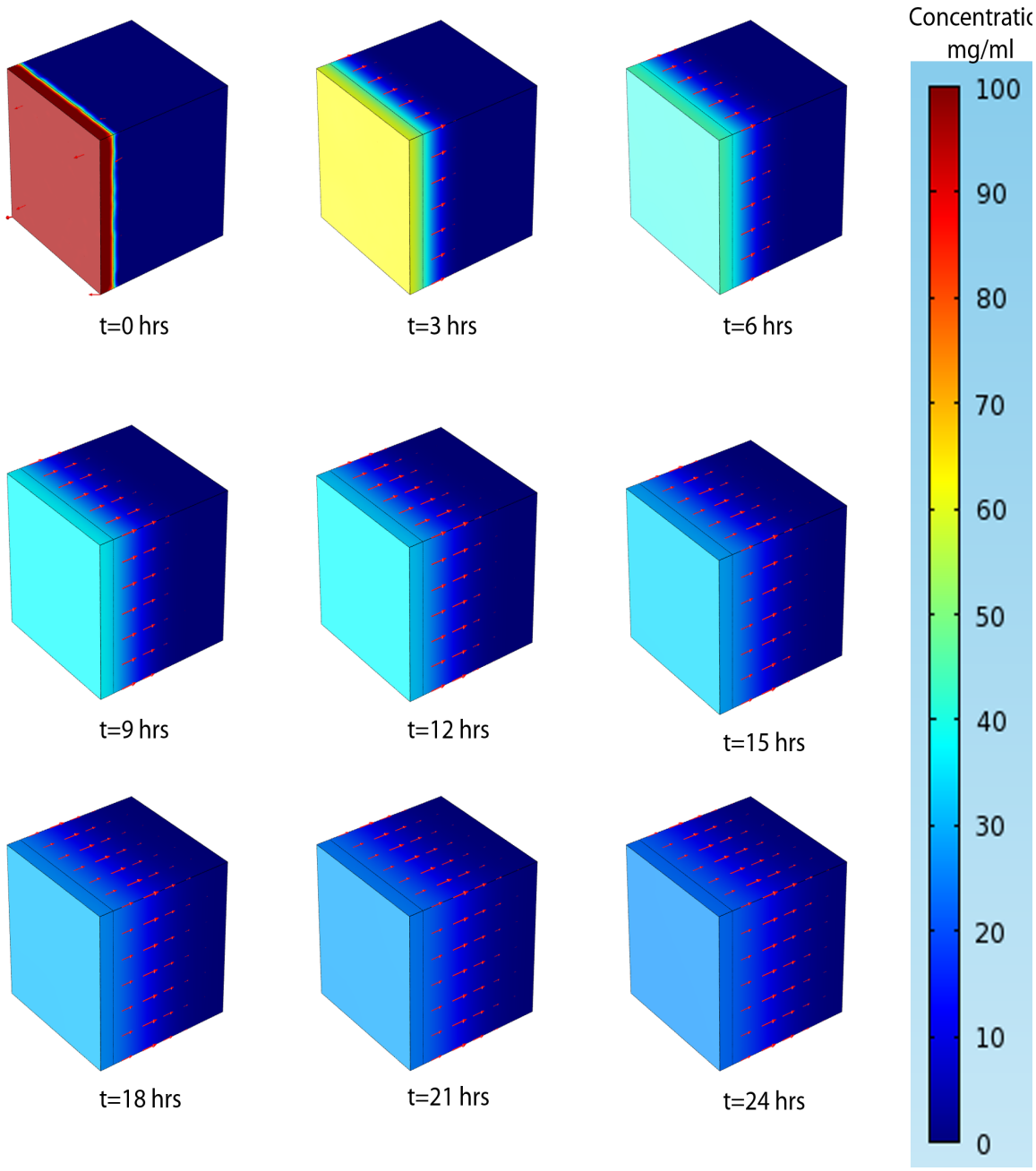


Figure 3.2 Diffusion of a molecule of 40nm hydrodynamic radius in a collagen block from an initial load of 100 mg/ml over a period of 24 hrs. Concentration level is shown in the color bar.

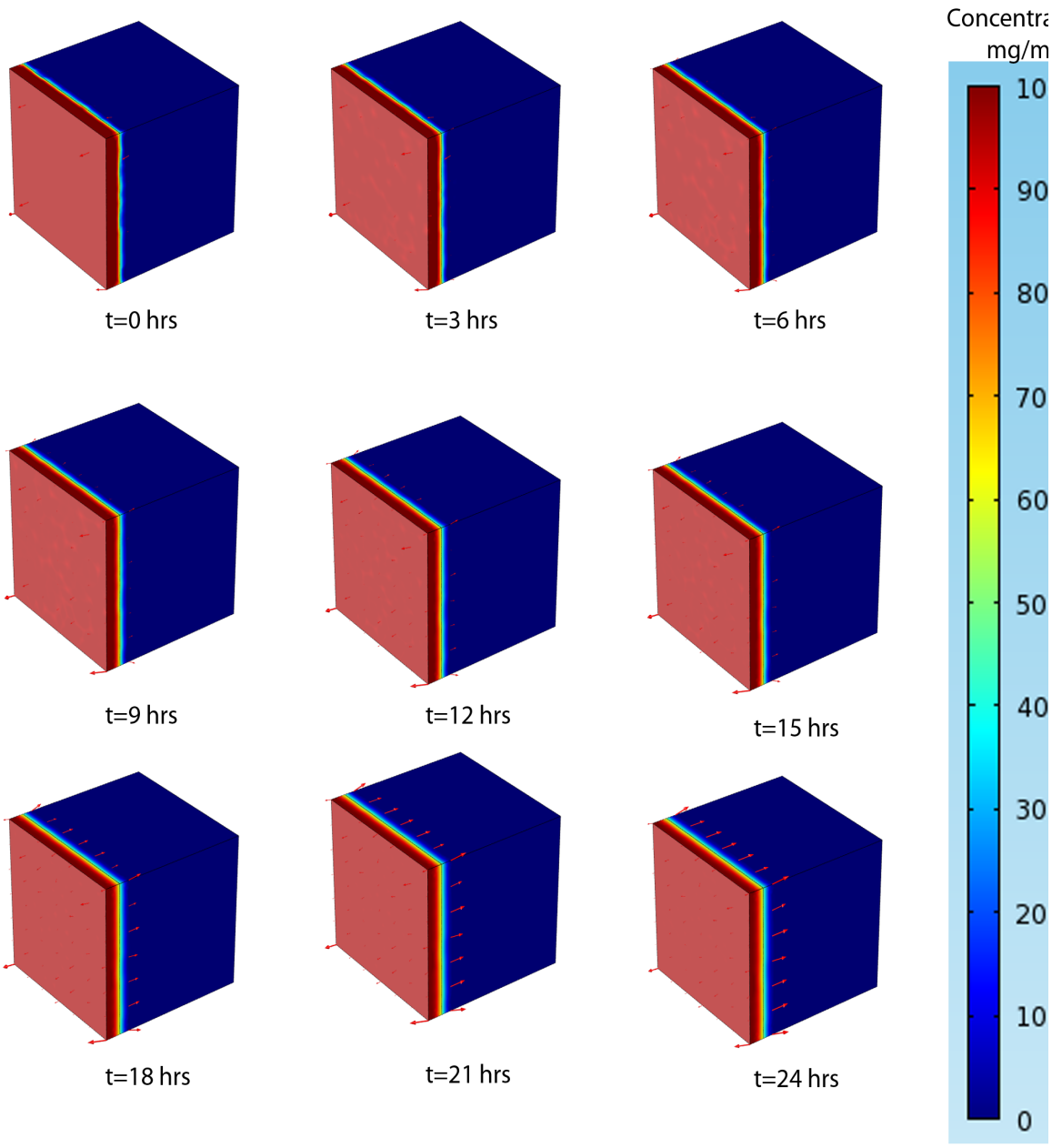


Figure 3.3 Diffusion of a molecule of 40nm hydrodynamic radius in an agarose block from an initial load of 100 mg/ml over a period of 24 hrs. Concentration level is shown in the color bar.

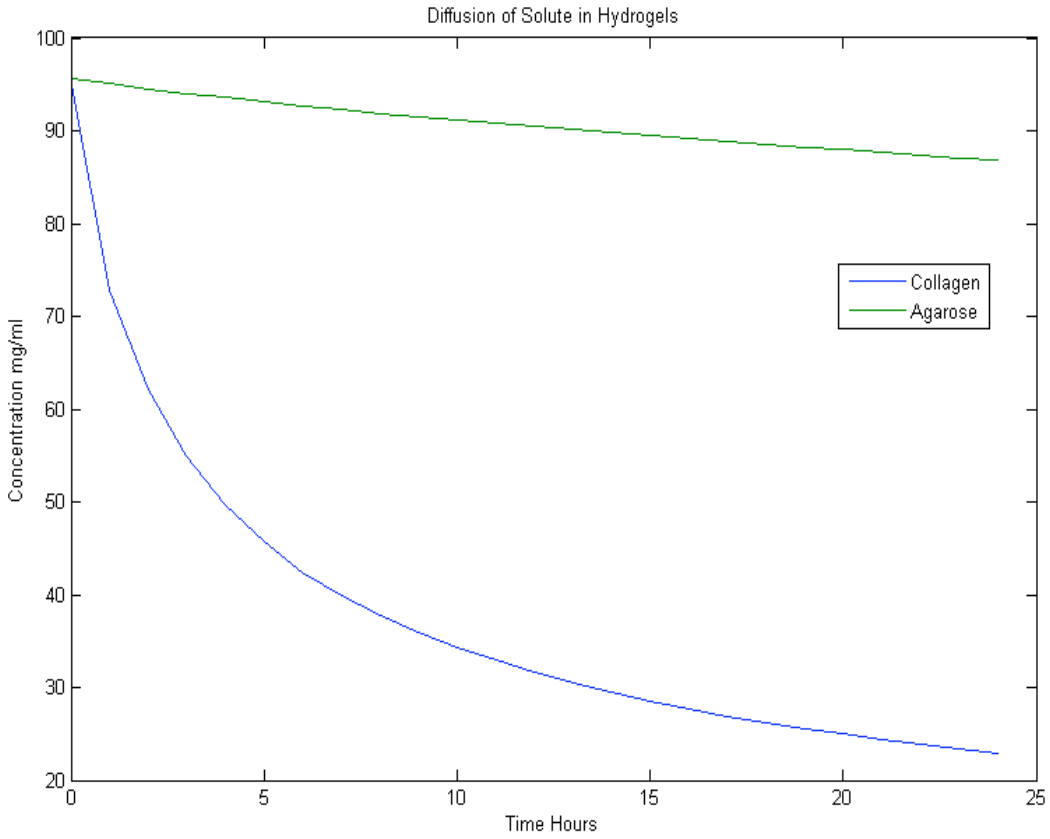


Figure 3.4 Comparison of the concentration decay from the original loaded volume from the collagen and agarose cubes modeled using the drug diffusion model.

The results summarized in figure 3.4 shows that the diffusion of the solute in agarose is considerably slower than the diffusion in collagen. The difference in the diffusion rate between the two polymers is a helpful characteristic for the development of a drug delivery system. It was expected that the diffusion in collagen would be considerably faster than the diffusion in agarose since the diffusion coefficient calculated for agarose was significantly smaller than the one calculated for collagen. However, the diffusion of the solute in a three-dimensional space was unknown. One of the significant findings of the simulation was the way the solute moved; a gradient was created directly adjacent to the location of the initial load. The formation of a gradient on the boundary of the loaded solute was more evident in agarose, since the diffusion was slower and the different concentration layers were observed.

## 3.2 Multimedium Drug Delivery System Model

### *3.2.1 Simulation Overview*

After the simulation of blocks with a single hydrogel present, multimedium models based on cylindrical nerve conduits with and without microchannels were implemented. The single channel and the multiluminal versions were modeled using an initial concentration of 100 mg/ml of a solute with the characteristics of a macromolecule of 40 nm in hydrodynamic radius. The diffusion coefficient was calculated to be 7.6 E -12 m^2/sec for collagen and 2.31 E -14m^2/sec for agarose.

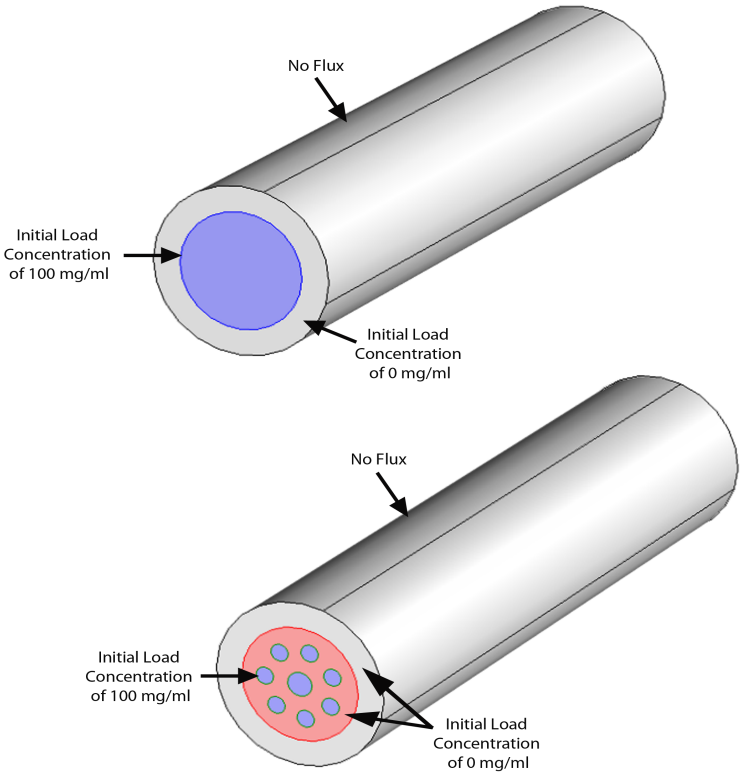


Figure 3.5 Boundary and initial conditions for the single and multiluminal configuration of the multimedium drug delivery model, shaded blue area shows the initial concentration of solute, the rest of the faces shown in gray represent no flux and region in red represents agarose content with no concentration of solute.

The concentration was loaded in the regions that contained collagen as shown in figure 3.5. The end caps of the cylinder were modeled as free flow boundaries, and the surface of the cylinder was modeled as a no flux boundary, as shown in figure 3.5, since the polymer utilized to make the outer tube of the nerve conduit devices is highly impermeable.

As in the previous study, the simulation was implemented and ran using COMSOL Multiphysics 4.0, and further simulation was ran using MATLAB 7.9.0 r2009b with the generated code in COMSOL. To ensure the reproducibility of the solution, the simulation was performed 5 times, each time the approximated solution was the same. A2.4 GHz Intel® Core™2 Quad processor computer was utilized during the simulations. The range of time considered for the simulation was 30 days, which took 25.52 seconds to compute the approximation for the single channel arrangement and 54.48 for the multiluminal arrangement. The time step utilized for the solution was every 6 hours, yielding a total of 121 time points for the simulation; however, the time step can be altered in order to find a specific time point. The increment in time points resulted in an increase in the solution computation time.

### *3.2.2 Simulation Results*

The result of the simulation for the single channel multimedium model is summarized in figure 3.5 and shows the change in concentration over time as well as the direction and magnitude of the diffusive flux of the solute. The change in concentration is depicted as a change in color specified by the colorbar shown in the same figure. The diffusive flux is shown as red arrows pointing in the direction of the flux and proportional in size to the magnitude. The average concentration of the lumen was monitored and shown in figure 3.9. The concentration changes along the length of the channel were also monitored.

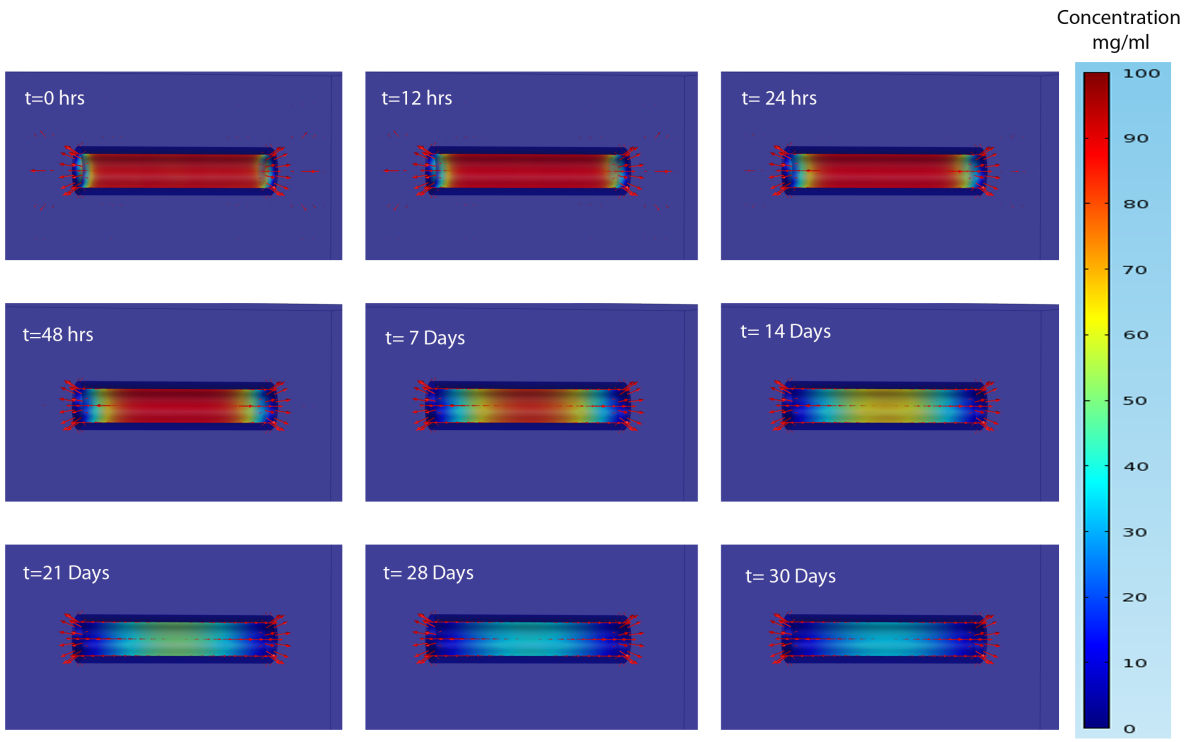


Figure 3.6 Diffusion of a molecule of 40nm hydrodynamic radius for the multimedium model with a single channel configuration with an initial load of 100 mg/ml over a period of 30 days. The concentration level is shown in the color bar. Diffusive flux is shown as red arrows proportional in size to the magnitude and oriented in the direction of the flux.

The results from the simulation show that the solute flow is bidirectional away from the center of the channel. The change in the concentration is evident at the ends of the cylinder, with the free flow boundary, where the flux is the highest. Fluxes in the center of the channel do not appear until the solute from the ends has diffused out; after that the solute from the center moves towards the region with higher flux. There is a big difference in the concentration between the center and the ends of the channel. For some time points the difference is as much as 40 mg/ml in1000 micrometers of the channel. During the first 12 hours of the simulation, the length of the uniform concentration in the center is about 9000 micrometers and drops to 4000 micrometers at 48 hours. Eventually the concentration in the center drops and the differences of the adjacent areas is reduced.

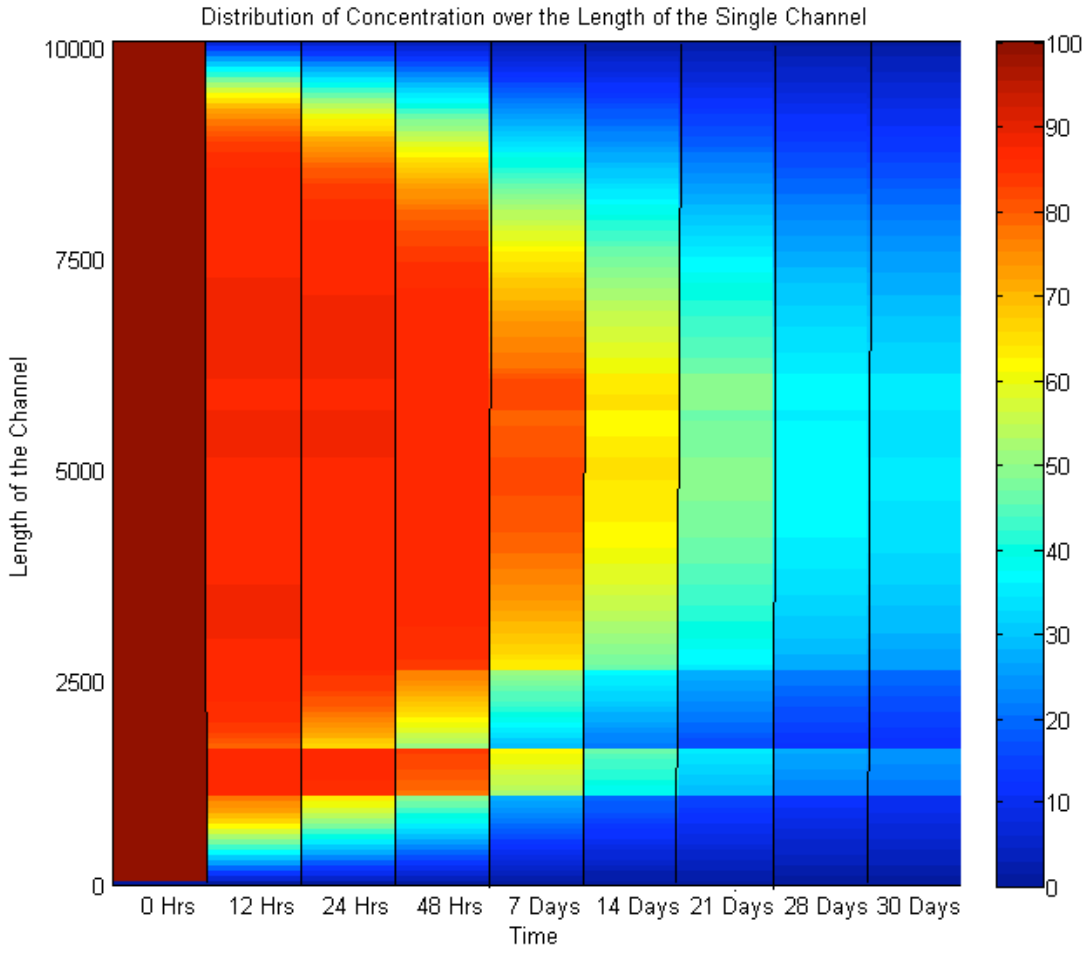


Figure 3.7 Change in concentration with respect to channel location over time for the single channel configuration.

When the multiluminal configuration was utilized for the simulation, the diffusive flux of the solute did not behave as in the single channel configuration. Instead, the flux moves in two directions, toward the end of the cylinders, and a smaller flux toward the agarose walls. The small flux toward the agarose was expected since the model follows Fick's law of diffusion and the diffusion in a medium is proportional to the diffusion coefficient. The result of the net flux in the microchannels resulted in a more uniform diffusion of the solute out of the microchannels, and a more stable environment throughout the microchannels. The diffusion behavior observed in the multiluminal arrangement is the product of two independent parameters: the volume of the channel, and the diffusion in the channels walls.

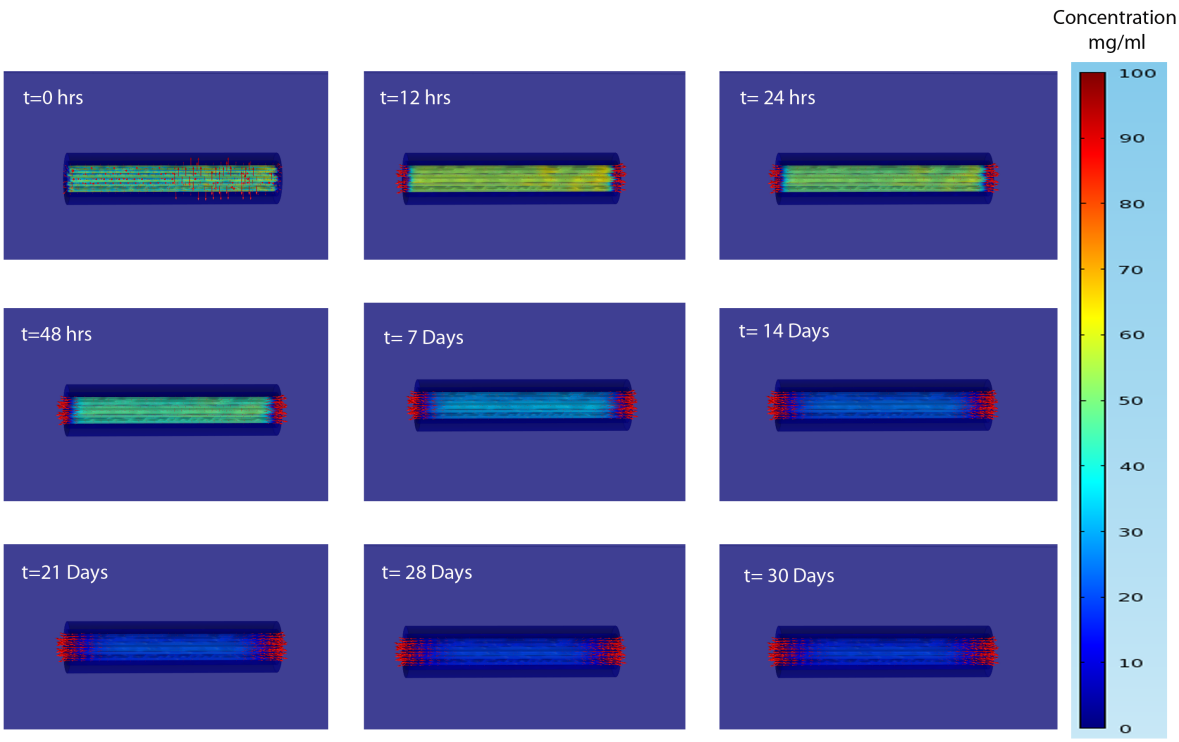


Figure 3.8 Diffusion of a molecule of 40nm hydrodynamic radius for the multimedium model with a multiluminal configuration with an initial load of 100 mg/ml over a period of 30 days. The concentration level is shown in the color bar. Diffusive flux is shown as red arrows proportional in size to the magnitude and oriented in the direction of the flux.

The concentration of solute in the microchannels was monitored. The solute distribution over the length of the microchannel for different time points is shown in figure 3.9. A steady concentration is kept along microchannels. There is a reduction in the homogeneous concentration length as time passes, but it is not as drastic as in the single channel arrangement. At one of the ends a fluctuation in the concentration appears that disappears as time progresses. However, the highest concentration in the channel drops lower than the highest concentration in the single channel.

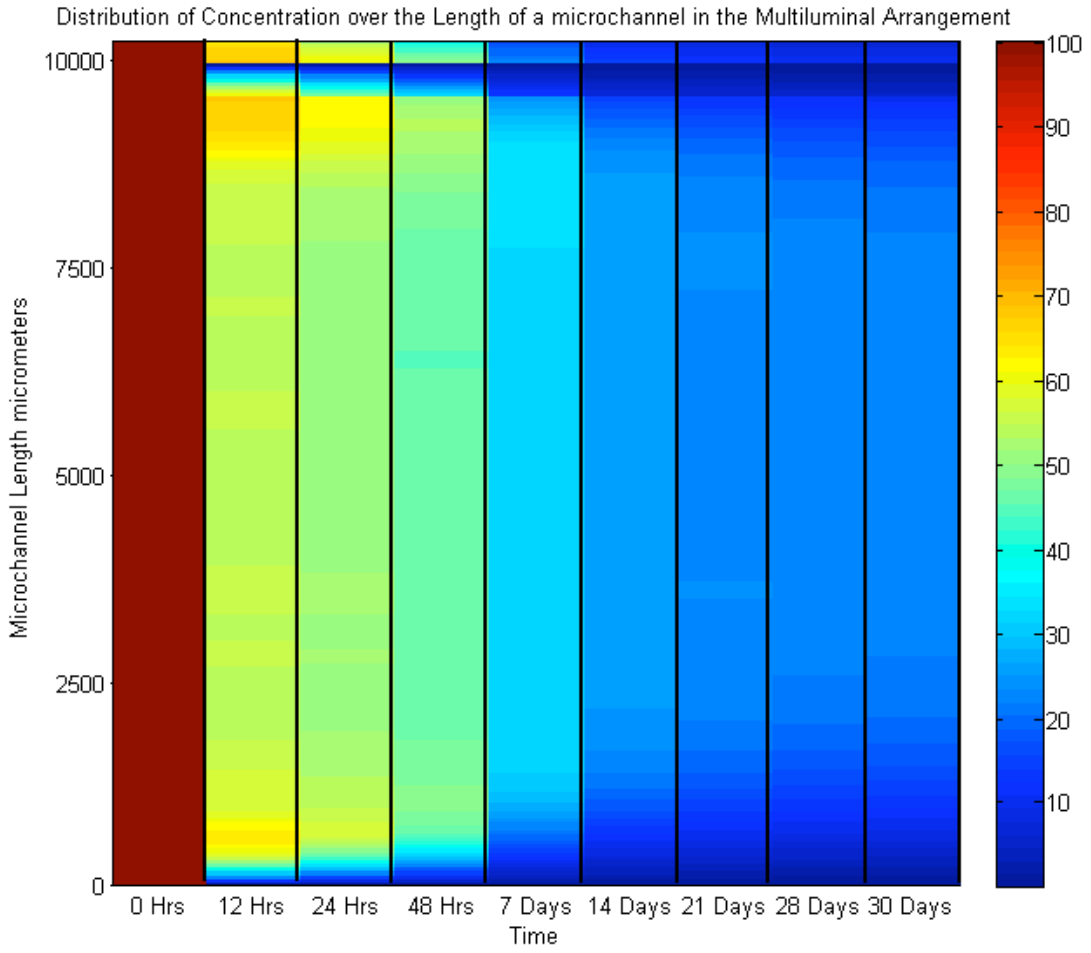


Figure 3.9 Change in concentration with respect to channel location over time for the multiluminal configuration

The average concentration for the single channel and the multichannel arrangement is summarized in figure 3.10. The average calculation only includes the initial loaded volume for both configurations. For the multiluminal arrangement, a concentration of solute is formed in the volume filled with agarose. Figure 3.10 show that the single channel configuration maintains a higher average concentration for the 30 days. However, the high concentration average is due to the lack of diffusion in the center of the channel, which remains at a high concentration for the entire 30 days.

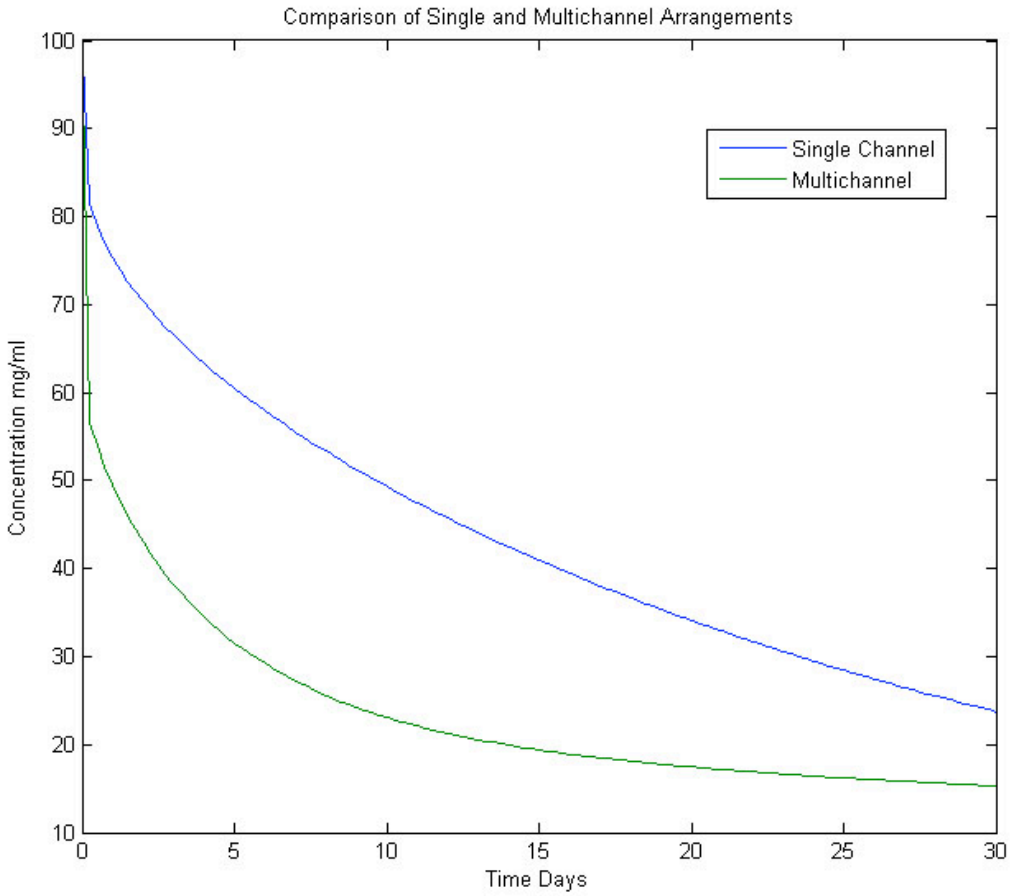


Figure 3.10 Comparison of the average concentration in the single and the multiluminal configurations of the multimedium model. The single and multimedium model based on nerve conduits utilized for peripheral nerve regenerations.

## 3.3 Incorporation of PLGA Microparticles Release to Multimedium Model

### *3.3.1 Implementation Overview*

In order to evaluate the advantage of the utilization of biodegradable polymers, release from PLGA microparticles was incorporated into both configurations of the multimedium model. Using the same protocol, the model was implemented and run in COMSOL Multiphysics using a 2.4 GHz Intel® Core™2 Quad processor computer. Due to large number of mesh elements in the model, the single channel configuration was loaded with 63 microparticles loaded with 35.1 E -6 grams, enough solute to create a concentration of 100 mg/ml for the entire volume of the channel. The release rate was modeled

using the derived release rate shown in the previous chapter. The simulation time range was set to 30 days as in the simulation for the multimedium model with the initial concentration load.

*3.32 Simulation Results*

The distribution of concentration is shown in figure 3.11; the change in concentration is depicted as a change in color specified by the colorbar shown in the same figure.

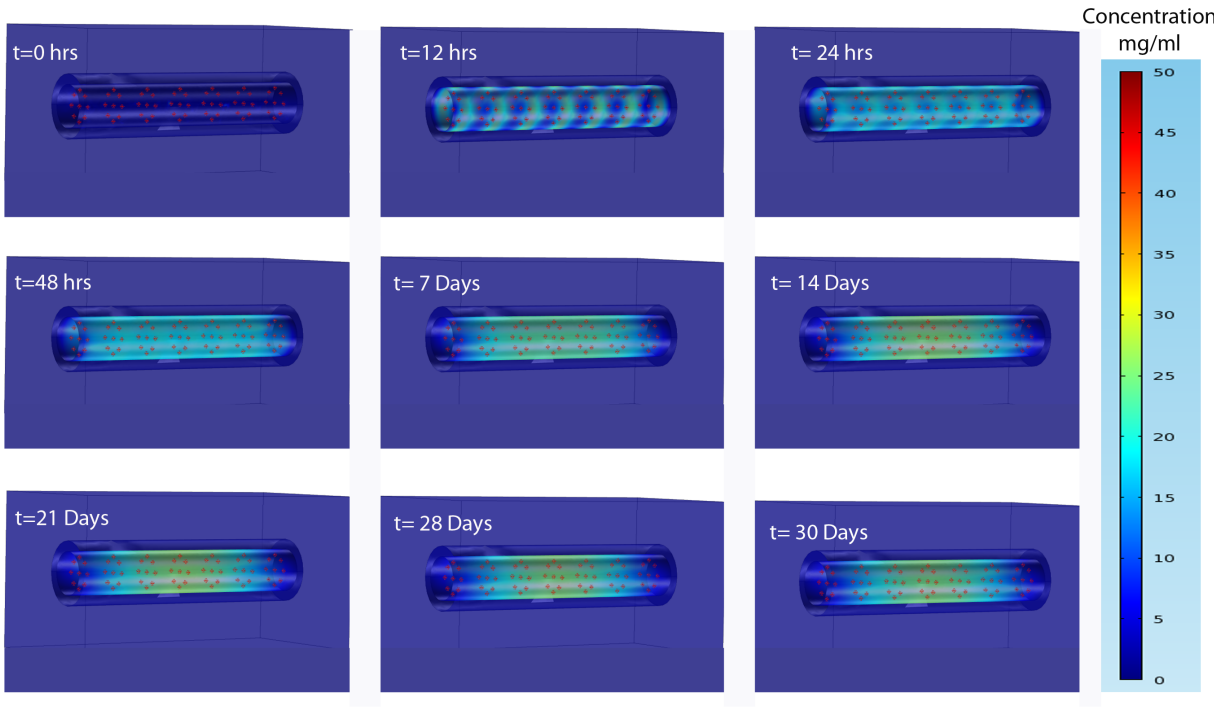


Figure 3.11 Diffusion of a molecule of 40nm hydrodynamic radius for the multimedium model with a single channel configuration with microparticles loaded with 35.1 E-6 grams. The concentration level is shown in the color bar.

The distribution of the concentration over the length of the microchannel is summarized in figure 3.12. Peaks of concentration are visualized during the first 12 hrs of the simulation, due to the initial burst of the PLGA microparticles. The initial burst and followed released is diffused throughout the channel, and the concentration becomes more uniform. After day 7 the solute concentrates in the center of the channel due to the increase of the diffusion out of the channel and the decrease of the release rate of the biodegradable polymer. The maximum concentration obtained with the loaded PLGA microparticles was 27 mg/ml from the first concentration peaks due to the initial burst release from the microparticles. A more

stable concentration could be obtained with the increase of loaded microparticles in the channel or the increase in the initial load of solute.

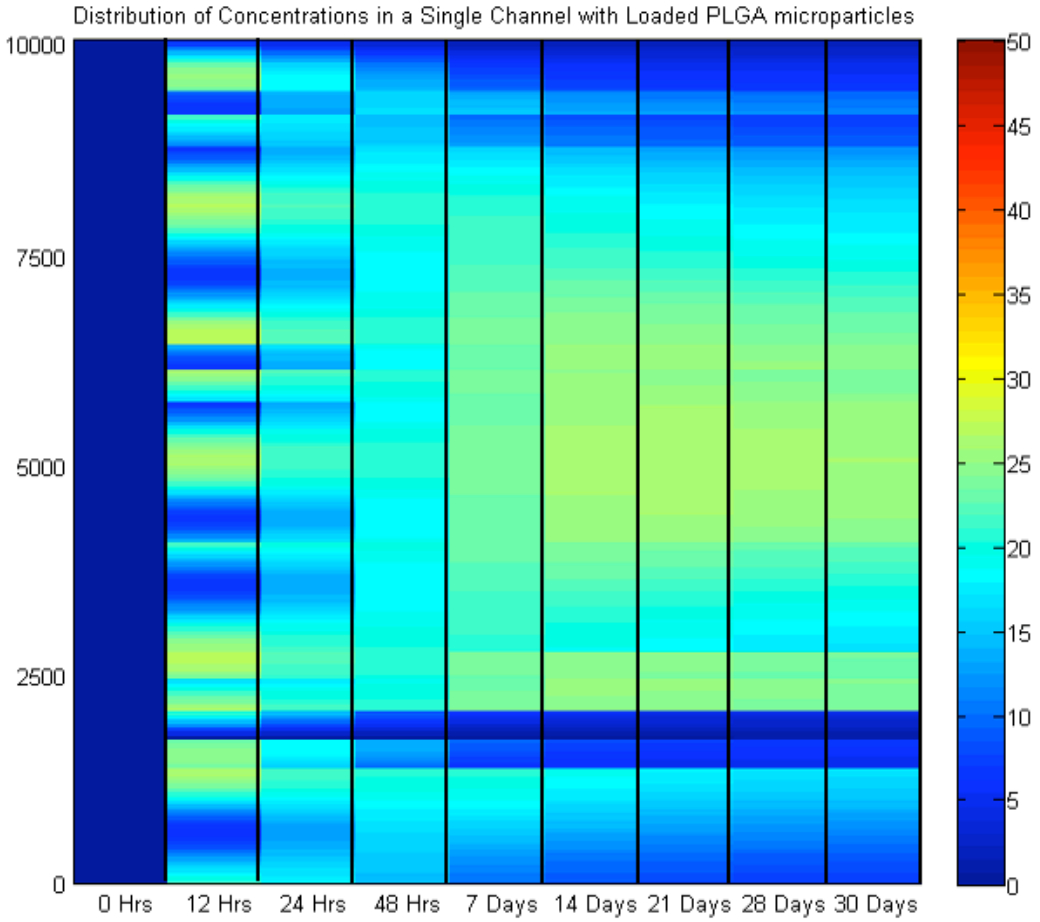


Figure 3.12 Change in concentration with respect to channel location over time for the single channel configuration with incorporated PLGA microparticles

The implementation of the multiluminal arrangement with PLGA microparticles was implemented using the same method utilized for the single channel configuration. Only the central microchannel in the device was modeled due to complex geometry and the high number of mesh elements created during mesh implementation. For the incorporation of PLGA microparticles in the multiluminal arrangement, the central microchannel was loaded with 55 microparticles, each particle loaded with 1.75 E-6 grams of solute. This

was sufficient to create a concentration of 100 mg/ml in the lumen of the microchannel. The release and diffusion profile over time is shown in figure 3.13, where the concentration of solute is depicted as a color level shown in the colorbar.

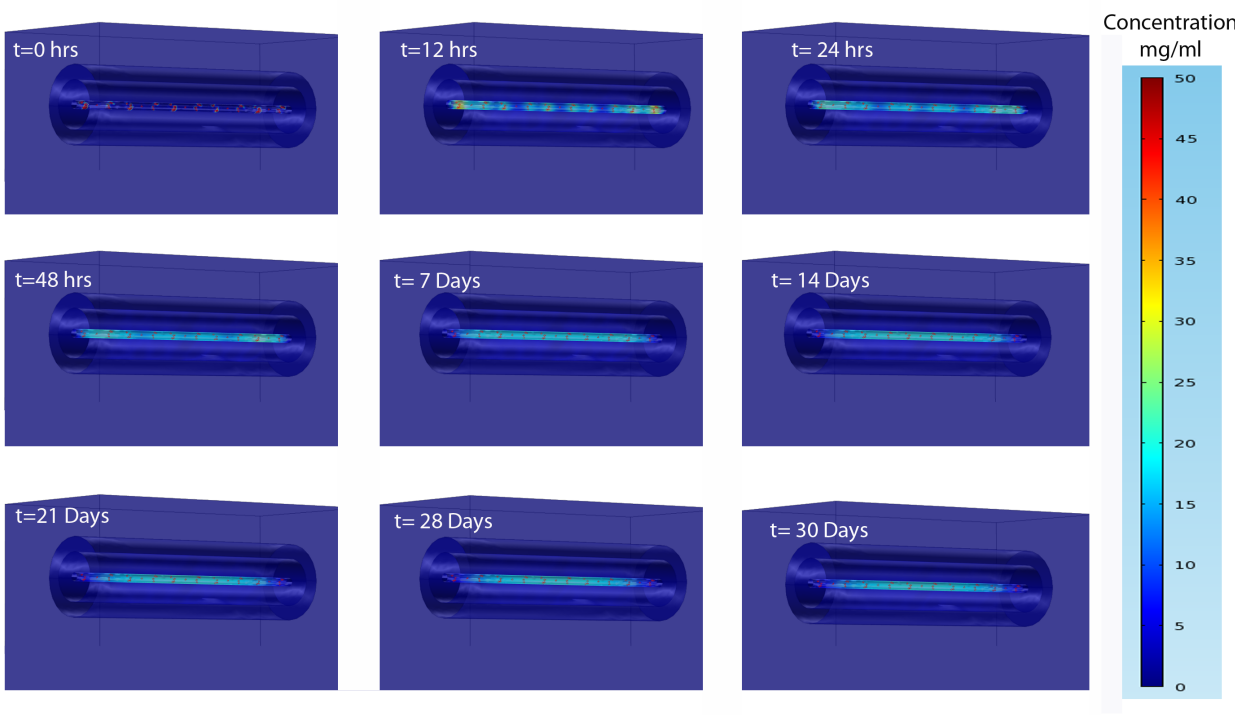


Figure 3.13 Release and diffusion profile of a molecule of 40nm hydrodynamic radius for the multimedium model with multiluminal configuration with microparticles loaded with 1.75 E-6 grams. The concentration level is shown in the color bar.

The solute concentration over the length of the microchannel was monitored and summarized in figure 3.14, which shows distribution of the solute within the microchannel for different time points. Compared with the single channel implementation with the PLGA microparticles, the concentration average is considerably lower. However, the range of length with uniform concentration is longer with a region close to 6000 micrometers compared with around 3000 micrometers of the single channel. This behavior can be attributed to the smaller volume and interaction of agarose in the microchannel walls as in the study with the solute loaded hydrogel.

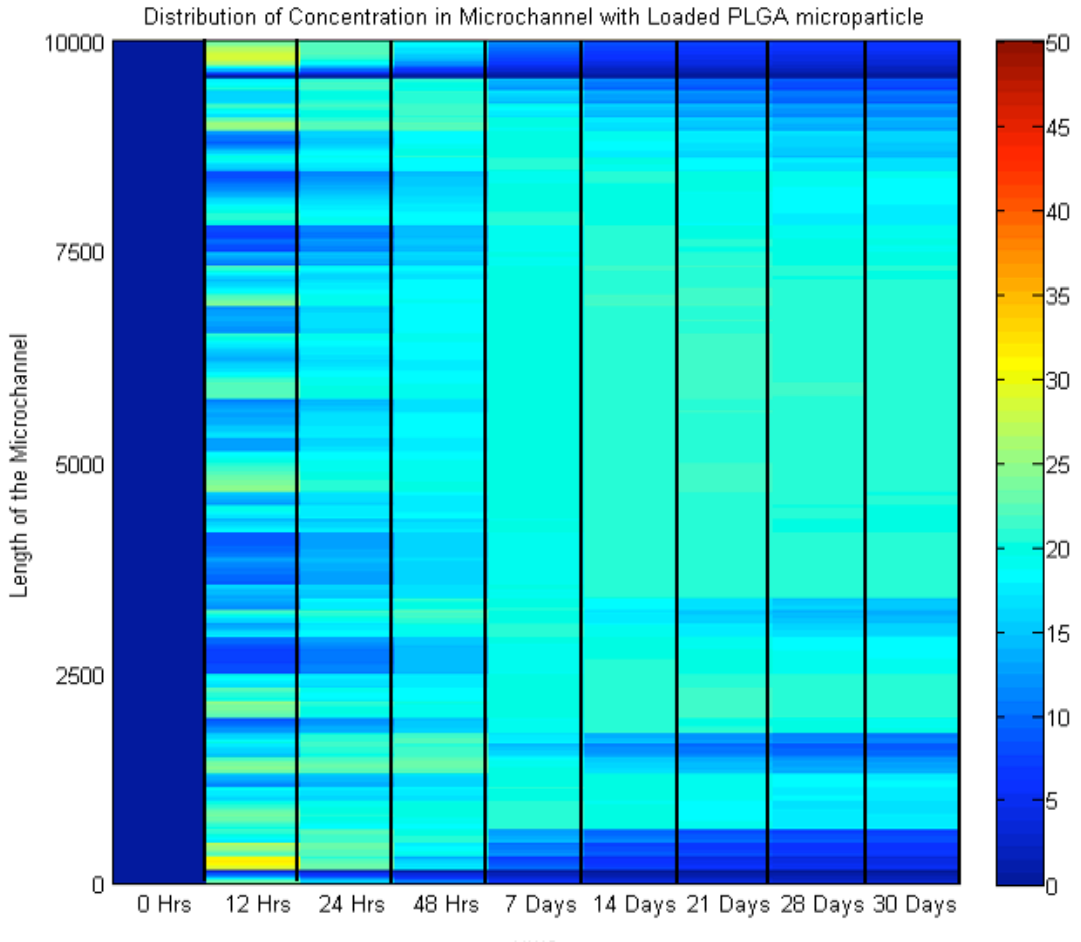


Figure 3.14 Change in concentration with respect to channel location over time for the multiluminal configuration with incorporated PLGA microparticles

The average concentration of solute in microchannels and in the single channel was measured, and summarized in figure 3.14. The average concentration for the single channel arrangement is higher than the microchannel due to the concentration retained in the center of the channel after the initial burst release. The accumulation of solute inside the single channel and the microchannel is a two step process: the release from the microparticles, and the diffusion out of the channel. For the microchannel, the solute starts diffusing out before a higher concentration of solute is reached. As the release rate of the polymer decreases, the average concentration decreases.

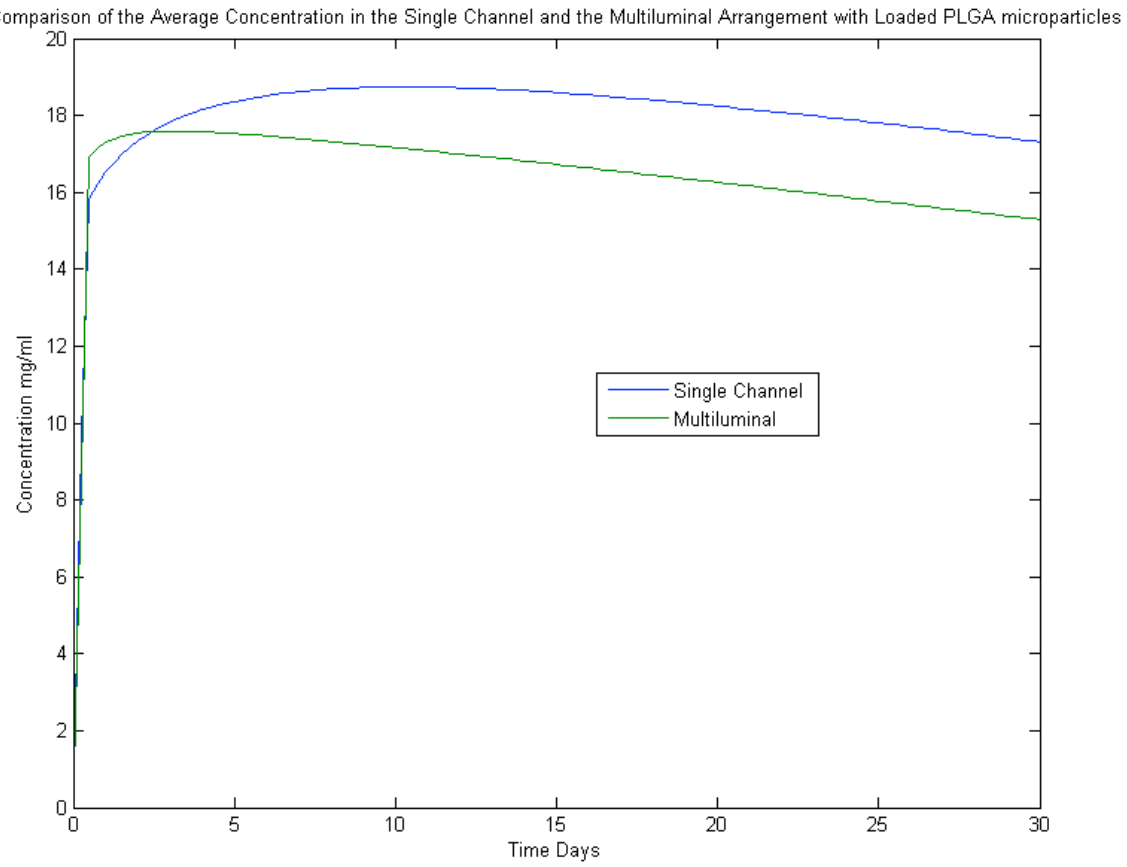


Figure 3.15 Comparison of the average concentration for 30 days in the single channel and multiluminal arrangements with loaded PLGA microparticles incorporated in the lumens.

## 3.4 Discussion

The results from the simulation show that the channels volume and diffusion coefficient are determining factors for the control of solute concentrations in the cylindrical scaffolds simulated in this study. Differences found in the distribution of solute can be exploited depending on the application. The concentration profile for the single channel arrangement showed that the concentration in the center of the channel remained higher and produced a concentration gradient from the center to the ends of the channel. Meanwhile the concentration distribution found in the multiluminal arrangement shows a more uniform distribution. When PLGA microparticles were utilized for the delivery of the solute into the channel, the concentration profile in the single channel formed a small gradient from the center of the

channel. Therefore, the greatest effect on the concentration profile was due to the volume of the channels.

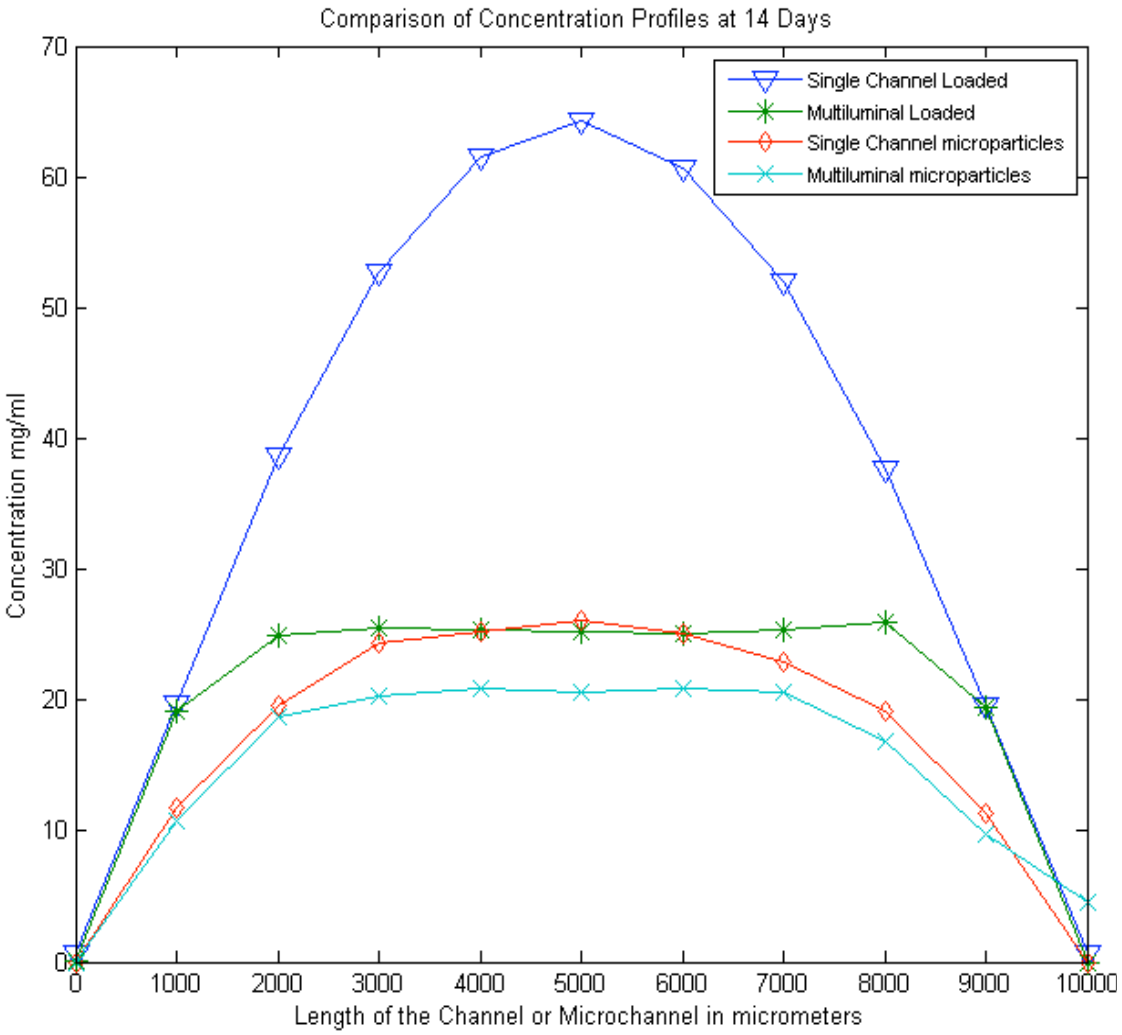


Figure 3.16 Concentration distribution over the length of the single channel and microchannels for all arrangements.

Figure 3.16 shows a summary of the concentration profiles for the four arrangements at 14 days. The characteristics of the release for the single channel configuration can be exploited for the bilateral regeneration of tissues such as in bone regeneration, vascularization, or migration of Schwann cells for nerve regeneration [43]. All the mentioned applications take advantage of the generation of gradients of

biomolecules for signaling mechanisms governing growth, migration, and differentiation of cells in living tissue[44]. Conversely, the utilization of multiluminal arrangements is more appropriate for the creation of a uniform concentration throughout the channel.

The delivery of biomolecules to support and promote regeneration of tissues is always a challenge due to the lack of control in their release [45, 46]. One example of the challenge is during the utilization of nerve conduits incorporating growth factors such as Nerve Growth Factor (NGF) to promote regeneration. During axonal regeneration, the growth of the axons is in one direction; therefore the higher concentration in the center could be inhibitory to growth [2]. Figure 3.17 illustrates the direction of Schwann cell migration when the single channel configuration is loaded with signaling molecules. Figure 3.18 shows the growth of axons in the multiluminal device when loaded with growth factors that promote axonal growth.

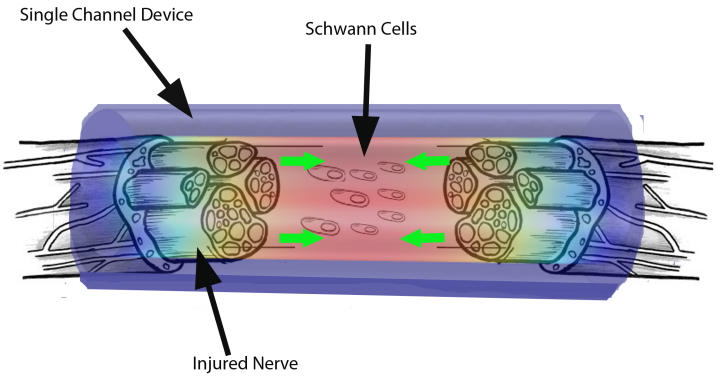


Figure 3.17 Implementation of the single channel device as a scaffold for peripheral nerve regeneration. Gradient formed in the device promotes the migration of Schwann cells to the center of the device, direction of migration shown as green arrows.

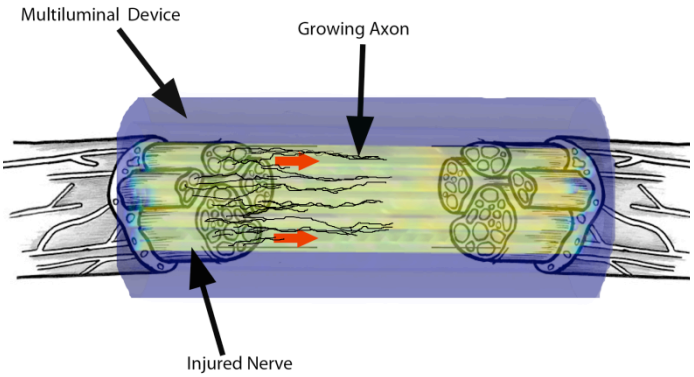


Figure 3.18 Implementation of the multiluminal device as a scaffold for peripheral nerve regeneration. Uniform concentration in the device promotes axonal nerve growth in one direction.

The simulations performed until now only provide clues to the internal microenvironment created in the cylindrical scaffold, but other applications for the simulation include the development of custom gradients for nerve regeneration using different degradable polymers. Advancement in computer technology will make possible the creation of more complex models that take into consideration more parameters and provide more realistic approximations.

We acknowledge that the multimedium model proposed in this work has some limitations and does not account for all the parameters involved in drug delivery. 1) Due to the limited computer power and the limitations in memory, the parameters that were taken into account for the model were only the major contributors to the release and the diffusion of the solutes in drug delivery. 2) Other parameters that affect diffusion and drug release like temperature and pH were considered as constant throughout the length of the simulation. The PLGA microparticles were assumed to be static and that they didn't move to within the scaffold. 3) The diffused molecule was assumed to have a spherical shape. However, we feel that the simulation produces a good approximation of the release and diffusion of solute within the device.

The multimedium model produced a description of the concentration profile within cylindrical scaffolds. In order to address limitations stated above future work will involve: 1) the utilization of a supercomputer to run the simulations involving more parameters. The incorporation of other parameters such as the degradation of the hydrogels, and its effect on the diffusion of the solute as well as the diffusion of the microparticles suspended in the lumen of the device will make the simulation more

accurate. 2) The validation using in vivo and in vitro experiments to validate results, since the validation performed to the model is purely theoretical, and based on in vitro experiments. The validation using an in vivo model will ensure that the approximation more reliable. Overcoming these limitations will establish a more complete computer model capable of optimizing available drug delivery systems, and the exploration different scaffold and polymer geometries to establish biological gradients ultimately providing the means to evaluate implantable scaffolds for different biomedical applications mentioned, before they are implanted.

## 3.5 Conclusion

Modeling of drug delivery systems has the potential to facilitate the development of new delivery methods and the understanding of the mechanism affecting the dosage and becomes an indispensable part of product development. Recently, the modeling of drug delivery systems has proliferated due to the importance of generating a numerical prediction for the system behavior during the design phase[47]. There are several theories established for drug release, but most are complicated and inaccurate [13]. When modeling, there is a balance between the accuracy and the number of phenomena to be taken into account, as considering too many parameters will make the model impractical.

The results from the simulations demonstrate that based on physical phenomena, the spatiotemporal concentration profiles of drug delivery devices can be approximated. The determination of the spatiotemporal concentration for drug delivery devices or scaffolds determines the functionality and efficacy of the system. Modeling the drug delivery system makes possible the optimization of the microenvironment created by the device. The control of the microenvironment within the lumen of the implantable device will ensure the released molecule has the desired biological effect to the targeted tissue.

Simulation of implantable drug delivery devices will contribute significantly to the development of tissue engineering, making possible the determination of the spatiotemporal concentrations of biomolecules that could not be determined otherwise. The control of microenvironments could lead to the improvement of the development of implantable scaffolds in the areas of angiogenesis, vascularization, and regeneration of nerve and bone, among others.

REFERENCES


1. Mark Saltzman, W., *Drug delivery: engineering principles for drug therapy*. 2001. p. 372.
2. Cao, X. and M.S. Shoichet, *Defining the concentration gradient of nerve growth factor for guided neurite outgrowth.* Neuroscience, 2001. **103**(3): p. 831-40.
3. Grassi, M. and G. Grassi, *Mathematical modelling and controlled drug delivery: matrix systems*, in *Current drug delivery*. 2005. p. 97-116.
4. Lao, L.L., S.S. Venkatraman, and N.A. Peppas, *Modeling of drug release from biodegradable polymer blends.* Eur J Pharm Biopharm, 2008. **70**(3): p. 796-803.
5. Lee, A.G., et al., *Development of macroporous poly(ethylene glycol) hydrogel arrays within microfluidic channels.* Biomacromolecules, 2010. **11**(12): p. 3316-24.
6. Houchin, M. and E. Topp, *Chemical degradation of peptides and proteins in PLGA: A review of reactions and mechanisms.* Journal of pharmaceutical sciences, 2008. **97**(7): p. 2395-2404.
7. Wu, X.Y. and Y. Zhou, *Finite element analysis of diffusional drug release from complex matrix systems. I complex geometries and composite structures.* J Control Release, 1997. **51**(1): p. 57-71.
8. Madenci…, E., *The finite element method and applications in engineering using ANSYS*, in *books.google.com*. 2006.
9. Panagiotopoulou, O., *Finite element analysis (FEA): applying an engineering method to functional morphology in anthropology and human biology*, in *Ann Hum Biol*. 2009. p. 609-23.
10. A. Truskey, G., F. Yuan, and D. F. Katz, *Transport phenomena in biological systems*. 2009. p. 860.
11. Carman, P., *Fluid flow through granular beds*, in *Chemical Engineering Research and Design*. 1937.

12. Kaunisto, E., et al., *A mechanistic modelling approach to polymer dissolution using magnetic resonance microimaging*, in *J Control Release*. 2010. p. 232-41.

13. Siepmann, J. and A. Göpferich, *Mathematical modeling of bioerodible, polymeric drug delivery systems*, in *Advanced drug delivery reviews*. 2001. p. 229-247.

14. Houchin, M. and E. Topp, *Chemical degradation of peptides and proteins in PLGA: A review of reactions and mechanisms*, in *Journal of pharmaceutical sciences*. 2008. p. 2395-2404.

15. Goodman, J., B. Thanoo, and P. DeLuca, *Identification of chemically modified peptide from poly (D, L-lactide-co-glycolide) microspheres under in vitro release conditions*, in *AAPS PharmSciTech*. 2003.

16. Rothstein, S., W. Federspiel, and S. Little, *A unified mathematical model for the prediction of controlled release from surface and bulk eroding polymer matrices*, in *Biomaterials*. 2009. p. 1657-1664.

17. Siepmann, J. and F. Siepmann, *Mathematical modeling of drug delivery*, in *International journal of pharmaceutics*. 2008. p. 328-343.

18. Siepmann, J., N. Faisant, and J.-P. Benoit, *A new mathematical model quantifying drug release from bioerodible microparticles using Monte Carlo simulations*, in *Pharm Res*. 2002. p. 1885-93.

19. Shoaib, M.H., et al., *Evaluation of drug release kinetics from Ibuprofen matrix tablets using HPMC*, in *Pak. J. Pharm. Sci*. 2006. p. 119-24.

20. Siepmann, J. and F. Siepmann, *Mathematical modeling of drug delivery.* International journal of pharmaceutics, 2008. **364**(2): p. 328-343.

21. Siepmann, J., et al., *Calculation of the dimensions of drug-polymer devices based on diffusion parameters*, in *Journal of pharmaceutical sciences*. 1998. p. 827-32.

22. Narasimhan, B., *Mathematical models describing polymer dissolution: consequences for drug delivery*, in *Advanced drug delivery reviews*. 2001. p. 195-210.

23. Frenning, G. and M. Strømme, *Drug release modeled by dissolution, diffusion, and immobilization*, in *International journal of pharmaceutics*. 2003. p. 137-145.

24. Zienkiewicz, O.C., *The Finite Element Method*. 3rd ed. 1977: McGraw-Hill Book Company.

25. Rao, S., *The finite element method in engineering*, in *books.google.com*. 2005.

26. Grassi, M. and G. Grassi, *Mathematical modelling and controlled drug delivery: matrix systems.* Current drug delivery, 2005. **2**(1): p. 97-116.

27. Faisant, N., J. Siepmann, and J. Richard…, *Mathematical modeling of drug release from bioerodible microparticles: effect of gamma-irradiation*, in *European Journal of …*. 2003.

28. Zhou, Y. and X. Wu, *Modeling and analysis of dispersed-drug release into a finite medium from sphere ensembles with a boundary layer*, in *Journal of Controlled Release*. 2003. p. 23-36.

29. Lao, L.L., S.S. Venkatraman, and N.A. Peppas, *A novel model and experimental analysis of hydrophilic and hydrophobic agent release from biodegradable polymers*, in *J Biomed Mater Res A*. 2009. p. 1054-65.

30. Lao, L.L., S.S. Venkatraman, and N.A. Peppas, *Modeling of drug release from biodegradable polymer blends*, in *Eur J Pharm Biopharm*. 2008. p. 796-803.

31. Charalambopoulou, G.C., et al., *Numerical and experimental investigation of the diffusional release of a dispersed solute from polymeric multilaminate matrices*, in *J Control Release*. 2001. p. 309-19.

32. Shaw, M. and A. Schy, *Diffusion coefficient measurement by the*, in *Biophysical journal*. 1981. p. 375-381.

33. Pluen, A., et al., *Diffusion of macromolecules in agarose gels: comparison of linear and globular configurations*, in *Biophysical journal*. 1999. p. 542-552.

34. Ramanujan, S., et al., *Diffusion and convection in collagen gels: implications for transport in the tumor interstitium*, in *Biophysical journal*. 2002. p. 1650-1660.

35. Wolfram, A., *Wolfram Mathematica Chemical Data.* 2011.

36. Narayanan, J., J.Y. Xiong, and X.Y. Liu, *Determination of agarose gel pore size: Absorbance measurements vis a vis other techniques*, in *Journal of Physics: Conference Series*. 2006. p. 83.

37. Huang…, X., *On the importance and mechanisms of burst release in matrix-controlled drug delivery systems*, in *Journal of Controlled Release*. 2001.

38. Fatin-Rouge, N., K. Starchev, and J. Buffle, *Size effects on diffusion processes within agarose gels.* Biophysical journal, 2004. **86**(5): p. 2710-2719.

39. Siepmann, J., et al., *A new model describing the swelling and drug release kinetics from hydroxypropyl methylcellulose tablets*, in *Journal of pharmaceutical sciences*. 1999. p. 65-72.

40. K.E. Tanseya, b., c, J.L. Seiferte, B. Bottermanf, M.R. Delgadod,g, *M.I. Romeroe., *Peripheral Nerve Repair Through Multi-Luminal Biosynthetic Implants.* 2011.

41. Dawood A.F., P.L., S.N. Dash, S.K.Kona, K.T. Nguyen, M.I. Romero, *VEGF Release in Multiluminal Hydrogels Directs Angiogenesis from Adult Vasculature in Vitro.* Cardiovascular Engineering and Technology, 2011.

42. J. Tarcha, P., *Polymers for controlled drug delivery*. 1991. p. 286.

43. Zhao, X., et al., *Directed cell migration via chemoattractants released from degradable microspheres.* Biomaterials, 2005. **26**(24): p. 5048-63.

44. Keenan, T.M. and A. Folch, *Biomolecular gradients in cell culture systems.* Lab Chip, 2008. **8**(1): p. 34-57.

45. Ungaro, F., et al., *Microsphere-integrated collagen scaffolds for tissue engineering: effect of microsphere formulation and scaffold properties on protein release kinetics.* J Control Release, 2006. **113**(2): p. 128-36.

46. Schmidt, C.E. and J.B. Leach, *Neural tissue engineering: strategies for repair and regeneration.* Annu Rev Biomed Eng, 2003. **5**: p. 293-347.

47. Witkowski…, W., *Two-dimensional finite element analysis of a polymer gel drug delivery system*, in *Materials Science and ….* 1995.

## BIOGRAPHICAL INFORMATION

Eduardo Martinez was born of Francisco Martinez and Maria del Rocio Sanchez on August 8th 1986 in San Luis Potosi, Mexico. At the age of 15 Eduardo and his family moved to Irving, Texas, where he attended high school. Upon graduation he took up studies at North Lake College to further his knowledge in Biology and mathematics. Wanting to pursue a career in medical imaging he joined the University of Texas at Arlington/University of Texas Southwestern Medical Center joint five year Biomedical Engineering program in August 2006. During his engineering training he developed an interest in neurology. In the summer of 2009 he had the opportunity to rotate in the Dr. Mario Romero-Ortega's neural-regeneration lab. During his rotation he was involved in a cerebral palsy study in collaboration with Scottish Rite Children's Hospital, eventually joining the neural regeneration lab full time. His ultimate goal is develop computer models that help the development of more dependable medical devices.